Wave Motion 54 (2015) 76–99

Contents lists available at ScienceDirect

Wave Motion

journal homepage: www.elsevier.com/locate/wavemoti

Theory and experiments on poro-acoustics with inner resonators

Claude Boutin [a,*], François Xavier Becot [b]

[a] Université de Lyon, Ecole Nationale des Travaux Publics de l'Etat, LGCB - CELYA - CNRS 5513, 69518 Vaulx-en-Velin Cedex, France

[b] Matelys 1 rue Baumer, 69120 Vaulx-en-Velin, France

HIGHLIGHTS

- Analytical model describing meta-porous media in local and global dynamic.
- Direct assessment of the wide low frequency band gap.
- Inner resonance results in an apparent negative gas compressibility.
- Experiments on prototypes evidence high absorption and dispersion at low frequency.
- The validated theory provides practical rules for realizing tunable meta-materials.

ARTICLE INFO

Article history:
Received 10 September 2014
Received in revised form 24 November 2014
Accepted 26 November 2014
Available online 12 December 2014

Keywords:
Acoustics
Meta-porous media
Helmholtz resonator
Homogenization
Experiments

ABSTRACT

The work proposed here deals with theory and experiment on the acoustics of gas saturated rigid porous media with inner resonance effects. First, we investigate the physics of porous media in which inner resonance phenomena occur. Then, through the homogenization method the macroscopic descriptions of (i) porous media constituted by a packing of Helmholtz resonators and of (ii) Helmholtz resonators embedded in a porous matrix are established. Around the eigen frequency of the resonator, the drastic change in the behavior of the medium results in band-gaps that can be determined analytically. Second, following the physical principles governing the inner resonance, several prototypes of such media are designed. Moreover, several extensions of this basic principle are described analytically and tested experimentally. Specific features of porous media embedding inner resonance effects are identified by common acoustic measurements and are shown to be in good agreement with the theory. Among the noteworthy results shown, it is confirmed experimentally that the resonators essentially modify the effective bulk modulus of the medium inducing strong velocity dispersion and high attenuation in the frequency range of the theoretical band gaps. In conclusion, we discuss the forthcoming applications of the macroscopic modeling, especially as a tool for designing new materials with unconventional properties such as large dissipation at low frequencies.

1. Introduction

This paper deals with theory and experiment on acoustics of gas saturated rigid porous media with inner resonance effects. Studies on heterogeneous media have shown that when a "partial" non equilibrium state occurs at the local scale, a

* Correspondence to: LGCB - CELYA - UMR CNRS 5513, Ecole Nationale des Travaux Publics de l'Etat, 69518 Vaulx-en-Velin Cedex, France. Tel.: +33 0 4 72 04 71 44; fax: +33 0 472 04 70 41.
E-mail address: claude.boutin@entpe.fr (C. Boutin).

http://dx.doi.org/10.1016/j.wavemoti.2014.11.013
0165-2125/

non-conventional behavior arises at the macroscopic scale. This is the case in highly contrasted elastic composite materials: the inner resonance of the soft constituent induces band gaps, as evidenced theoretically in the pioneer paper [1] (see also [2]), and demonstrated in practice by [3] or [4,5]. An other example is the transient inner diffusion phenomenon in double porosity media [6,7] experimentally evidenced in poro-acoustics [8,9]. Weakly damped resonance (elasto-inertial effects) or strongly damped resonance (transient diffusion mechanisms) yield different macroscopic behavior e.g. with or without band gaps respectively. However, in both cases the macroscopic description strongly departs from usual modeling. Such materials constitute a particular class of "metamaterials", and are of prime interest for their unconventional properties, that are seemingly impossible to reach with classical materials.

The coexistence of dynamic phenomena at both the microscopic and macroscopic scales only occurs with specific microstructural configurations and in particular frequency range(s). We will focus here on the case where, under the "co-dynamic" regime, one distinguishes within any Elementary Representative Volume (ERV) a domain that experiences a dynamic state, while the complementary domain experiences a "quasi-static" state. This situation has several advantages that will be exposed throughout the paper: (1) it makes possible a simple modeling, (2) it corresponds to configurations much relevant in practice, (3) it includes the essential of the physics. To reach such situation, the ERV's constituents must present highly contrasted properties, otherwise they will experience a similar regime associated with a common wavelength. This contrast may result either through physical parameters of different order of magnitude (as in the examples mentioned above), or through morphological contrasts as in reticulated media [10] or in the present study. Indeed, it was established in [11,12], (see also [13]) that a "co-dynamic" regime may appear in "ad-hoc" designed periodic array of Helmholtz resonators embedded in a porous matrix. The present paper proposes modeling of such media and experimental validations of the main theoretical outcomes.

The paper is structured as follows. First, we investigate the physics of heterogeneous porous media in which inner resonance phenomena occur. To reflect the physics of the phenomena, and conversely to usual cases, different scaling and expansions are used in different regions of the gas. Such situations can nevertheless be addressed through the two-scale homogenization method [14,15]. Hence the macroscopic descriptions of (i) porous media constituted by a packing of Helmholtz resonators and of (ii) Helmholtz resonators embedded in a porous matrix (see Fig. 1) are established. Several generalizations based on other configurations (multiple resonators at distinct frequency, quarter wavelength resonators, "parabolic" microporous resonators) are also presented. Second, following the physical principles governing the inner resonance, several prototypes of such media are designed. Their specific features are identified by common acoustic measurements and are shown to be in good agreement with the theory. Among notable results, it is confirmed experimentally that the resonators essentially modify the effective stiffness of the gas that in turn induces strong dispersion in the frequency range of band-gaps identified theoretically. In conclusion, we discuss the forthcoming applications of the macroscopic modeling, especially as a tool for designing new materials with unconventional properties.

2. Theoretical models

We consider heterogeneous porous media presenting a statistically invariant representative volume element, that are conveniently represented by periodic media of period $\widehat{\Omega}$ and characteristic size ℓ, (Fig. 2). The study focuses on the description of particular media in co-dynamic regime i.e. when the propagation of long waves coincides with the resonance of a component of the period. Thus, in the usual sense of homogenization [14,15], a scale separation exists between the period size and wavelength.

2.1. Homogenization method

We are interested in wave propagation with a wave-length Λ much longer than the size ℓ of the period. The presence of the scale separation enables us to use the asymptotic multiple scale homogenization method to derive the equivalent macroscopic behavior. We denote by $L = \Lambda/2\pi$ the macroscopic characteristic length of the wave, and by ε the scale ratio parameter $\varepsilon = 2\pi\ell/\Lambda = \ell/L \ll 1$. To represent the two scales of the co-dynamic regime, one introduces two sets of dimensionless space variables, $\mathbf{x}/\ell = \mathbf{y}^*$ and $\mathbf{x}/L = \mathbf{x}^*$ associated respectively to the variations at the period and at the wave-length scales, where $\mathbf{x}$ stands for the usual space variable. Equivalently, taking L as reference length, two space variables, $\mathbf{y} = L\mathbf{y}^* = \varepsilon^{-1}\mathbf{x}$ and $\mathbf{x} = L\mathbf{x}^*$ will be used, the usual derivative being therefore changed into $\varepsilon^{-1}\partial/\partial y + \partial/\partial x$. The homogenization process is achieved accordingly to [14,15]. The field variables are expanded in power of ε, each term (specified by exponents in brackets) being $\widehat{\Omega}$ periodic. For example, the pressure p reads:

$$p(\mathbf{x}, \mathbf{y}) = \sum_0^\infty \varepsilon^i \, p^{(i)}(\mathbf{x}, \mathbf{y}). \tag{1}$$

To reflect the physics of the phenomena, the use of asymptotic expansions is combined with a rescaling of the equations based upon the dimensional analysis. This procedure ensures that the limit description obtained when $\varepsilon \to 0$ keeps a physic of the same nature as in the real situation where the scale separation is finite. The specificity of homogenization in presence of Helmholtz resonators is that the "contrast of geometry" implies introducing different scalings and expansions in different regions of the gas domain.

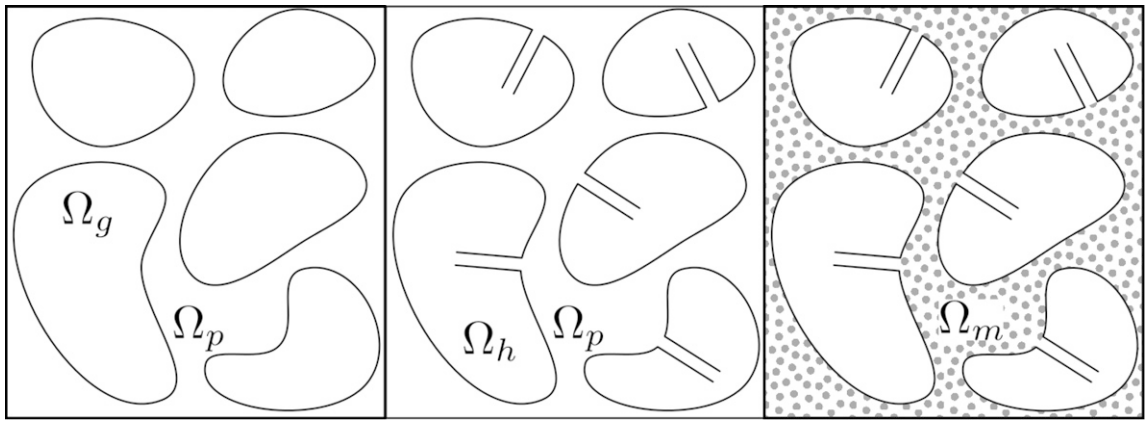

Fig. 1. Illustration of the different models considered. From left to right: impervious spheres in air (Section 2.2), resonators in air (Section 2.3), resonators in porous medium (Section 2.4). Experiments on the three configurations are reported in Section 4.

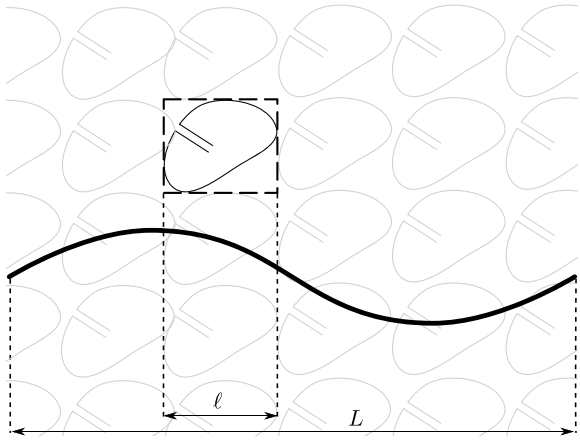

Fig. 2. Pattern of the periodic medium containing inner resonators.

Then, these expansions are introduced in the equations written with the two-scale derivatives and rescaled according to the physical analysis. The terms of the same power in ε are then identified, and the problems obtained in series are solved until the equation governing the phenomena at the leading order is obtained.

For conciseness, in this paper we highlight the rescaled formulations reflecting the physics and give the corresponding macroscopic descriptions without detailing the homogenization process.

In the sequel, we study small acoustic perturbations from the equilibrium state. The analysis is performed in the Fourier space with harmonic time dependence $\exp(+i\omega t)$ where ω and $f = \omega/2\pi$ are the angular frequency and the frequency. By linearity the time dependence is generally omitted. We consider porous media saturated by air (or any other gas), whose ambient pressure, temperature and density at equilibrium are respectively P^e, T^e and ρ^e; the physical parameters are, the viscosity μ, the heat mass capacity c_p, the heat capacity ratio γ, the heat conduction κ (recall that $c_p(1-\frac{1}{\gamma}) = \frac{P^e}{T^e\rho^e}$). The sound velocity is denoted $\mathcal{C}^e = \sqrt{\gamma P^e/\rho^e}$. For air in ambient conditions, $P^e = 1.013 \times 10^5$ Pa, $\rho^e = 1.2$ kg/m^3, $\gamma = 1.4$, $\mu = 1.84 \times 10^{-5}$ Pa · s, $\kappa = 0.026$ W/(m · K), $c_p = 1019$ J/(kg · K) and $\mathcal{C}^e = 343$ m/s.

2.2. Conventional porous media

Let us briefly recall the reference poro-acoustic theory, by considering porous media made of a packing of impervious grains. As illustrated in Fig. 1, the characteristic size of the grains and of the pores is of the order of the size ℓ of the period $\widehat{\Omega} = \Omega_p \cup \Omega_g$ where Ω_p and Ω_g denote respectively the pore and grain domains of interface Γ. The porosity is $\phi_p = |\Omega_p|/|\widehat{\Omega}| = 1 - |\Omega_g|/|\widehat{\Omega}|$.

2.2.1. Physics of the gas in the pores and rescaled equations

In the pores Ω_p, the linearized equations governing the harmonic perturbations, are given below where p_p, ρ_p, θ_p, stand respectively for the perturbations of pressure, density, and temperature, while $\mathbf{v}_p$, $\mathbf{D}(\mathbf{v}_p)$ denote the velocity and the strain

rate. The set of equations is constituted by the gas mass balance, the Navier–Stokes equation (momentum balance), Fourier equation (energy balance), and the state equation of the gas:

$$\mathrm{div}(\mathbf{v}_p) + i\omega\frac{\rho_p}{\rho^e} = 0 \tag{2}$$

$$\mu\mathbf{div}(\mathbf{D}(\mathbf{v}_p)) - \nabla p_p - i\omega\rho^e\mathbf{v}_p = \mathbf{0} \tag{3}$$

$$\mathrm{div}(\kappa\nabla\theta_p) - i\omega(\rho^e c_p\theta_p - p_p) = 0 \tag{4}$$

$$\frac{p_p}{P^e} = \frac{\rho_p}{\rho^e} + \frac{\theta_p}{T^e}. \tag{5}$$

On the gas–solid interface Γ, the boundary conditions are the adherence condition and the isothermal condition on the solid:

$$\mathbf{v}_p = \mathbf{0}; \qquad \theta_p = 0. \tag{6}$$

From the state equation, the pressure and temperature are kept as independent variables while the gas density ρ is expressed in function of the two previous variables. In the pores, the viscous shear stresses and the heat flux vary at the local scale while the pressure varies at the macroscale. Consequently, when re-expressed with the $(\mathbf{x}, \mathbf{y})$ variables (remind that L is the reference length), the terms $\mu\mathbf{div}(\mathbf{D}(\mathbf{v}'))$ and $\mathrm{div}(\kappa\nabla\theta_p)$ have to be rescaled as $\mu(\ell/L)^2\mathbf{div}(\mathbf{D}(\mathbf{v}')) = \mu\varepsilon^2\mathbf{div}(\mathbf{D}(\mathbf{v}'))$ and $\varepsilon^2\mathrm{div}(\kappa\nabla\theta_p)$. Thus, the "$x$–$y$-rescaled" Navier–Stokes equation takes the following form:

$$\mu\varepsilon^2\mathbf{div}(\mathbf{D}(\mathbf{v}_p)) - \nabla p_p - i\omega\rho^e\mathbf{v}_p = \mathbf{0} \tag{7}$$

$$\varepsilon^2\mathrm{div}(\kappa\nabla\theta_p) - i\omega(\rho^e c_p\theta_p - p_p) = 0. \tag{8}$$

Remark. The ε^2-scaling applies to the differential operator $\mathbf{div}(\mathbf{D}(-))$ re-expressed with the $(\mathbf{x}, \mathbf{y})$ variables. For this reason the parameters μ and κ are unchanged compared to the single variable formulation ((3)–(4)).

2.2.2. Conventional poro-acoustics – a reminder

The homogenization process leads successively to the following well known results [16–19], or [7]. First it is established that the pore's pressure varies at the macroscale i.e. $p_p^{(0)}(\mathbf{x}, \mathbf{y}) = P^{(0)}(\mathbf{x})$. Second, under the forced macroscopic pressure gradient, the periodic visco-inertial flow around the impervious grains leads to the dynamic Darcy law. Similarly, in the gas in contact with the grains (in isothermal state), the heat transfer forced by the macroscopic pressure leads to the temperature and density periodic distribution. Then, the global mass balance on the whole cell provides the effective bulk modulus that accounts for the non uniform temperature through the "thermal function" denoted hereafter $\Pi_p(\omega)$. This function defined in [7] using homogenization, is related to the dynamic thermal permeability $K_p'(\omega)$ introduced in [20]: $\Pi_p(\omega) = \frac{\gamma-1}{\gamma}\frac{i\omega\rho^e c_p}{\kappa}\frac{K_p'(\omega)}{\phi}$.

This results in a set of equations, where the derivatives are taken according to the macro space variable and the pressure and the mean flux are the leading order terms $P^{(0)}$, $\mathbf{V}^{(0)}$. For this reason, the index $_x$ indicating the derivative and the exponent $^{(0)}$ indicating the order can be dropped without ambiguity. Thus the macroscopic description reads, where $\mathbf{V}$ is the integral of the velocity in the pores, divided by the total cell volume and P is the pore pressure:

$$\mathrm{div}(\mathbf{V}) + i\omega\frac{P}{P^e}\phi_p[1 - \Pi_p(\omega)] = 0 \tag{9}$$

$$\mathbf{V} = -\frac{K_p(\omega)}{\mu}\nabla P = -\frac{\phi_p}{i\omega\rho^e\tau_p(\omega)}\nabla P.$$

In these equations, for simplicity, the medium is assumed macroscopically isotropic so that the dynamic permeability tensor and the dynamic tortuosity tensor reduce to scalar functions $K_p(\omega)$, $\tau_p(\omega)$ related by the equalities:

$$\rho^e\tau_p(\omega) = \frac{\mu\phi_p}{i\omega K_p(\omega)}.$$

The dynamic permeability K_p, and the effective bulk modulus of the gas $E_p = \frac{P^e}{\phi_p}\frac{1}{1-\Pi_p}$, are complex and frequency dependent. At low frequencies, the flow is governed by the viscosity then, $K_p \to \mathcal{K}_p$, the real-valued intrinsic permeability ; and the perturbation is quasi-isotherm i.e. $E_p \to P^e/\phi_p$. At high frequencies, the flow is governed by the inertia then $K_p \to (\phi_p\mu)/(i\omega\rho^e\alpha_{p_\infty})$ where α_{p_∞} will be called by convention the tortuosity (throughout the paper this term is reserved for the high frequency limit of the dynamic tortuosity); and the perturbation is quasi-adiabatic thus $E_p \to \gamma P^e/\phi_p$. Low and high frequency domains are delimited by the critical frequency ω_c derived by equalizing the low frequency viscous effects and the high frequency inertial effects ; the isothermal/adiabatic transition occurs at a frequency $\omega_t \approx O(\omega_c)$:

$$\omega_c = \frac{\phi_p\mu}{\mathcal{K}_p\rho^e\alpha_{p_\infty}}.$$

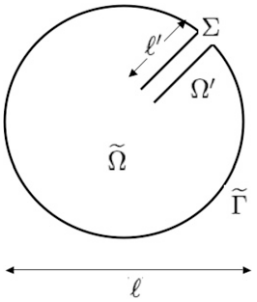

Fig. 3. Example of spherical Helmholtz resonator of volume $\Omega_H = \widetilde{\Omega} \cup \Omega'$.

Eliminating the flux $\mathbf{V}$ gives the wave equation and its corresponding wavelength:

$$\frac{P^e}{1-\Pi_p(\omega)}\Delta P + \omega^2 \rho^e \tau_p(\omega) P = 0 \qquad \frac{\Lambda_p(\omega)}{2\pi} = \frac{1}{\omega}\sqrt{\frac{P^e}{\rho^e}\frac{1}{\tau_p(\omega)(1-\Pi_p(\omega))}}. \tag{10}$$

Hence, at low frequency ($\omega \ll \omega_c$) the wave if of parabolic type and $|\frac{\Lambda_p}{2\pi}| \approx \frac{1}{\sqrt{\omega}}\sqrt{\frac{P^e \mathcal{K}_p}{\mu \phi_p}}$, while at high frequency ($\omega \gg \omega_c$) it becomes of hyperbolic type and $|\frac{\Lambda_p}{2\pi}| \approx \frac{1}{\omega}\frac{c^e}{\sqrt{\alpha_{p\infty}}}$. This modeling is valid when the scale separation assumption is satisfied, i.e. in the frequency range lower than the diffraction frequency defined by:

$$\omega \ll \omega_d; \qquad \frac{\Lambda(\omega_d)}{2\pi} \approx \ell.$$

2.3. Porous media made of resonators

In this section we consider a periodic medium similar as in the previous section, except that the impervious grains are now replaced by Helmholtz resonators (see Fig. 1(b)). Thus, the characteristic size of the resonators and of the pores (delimited by the interspace between the resonators) is of the order of the size ℓ of the period $\widehat{\Omega}$. For simplicity, the period is assumed to contain a single Helmholtz resonator Ω_H (thus the resonators are all identical) that does not intercept the boundary $\partial\widehat{\Omega}$ of the period. Ω_p and Ω_H denote respectively the pores domain and the volume of the resonator and we have $\widehat{\Omega} = \Omega_p \cup \Omega_H$. The concentration of resonators is $c = |\Omega_H|/|\widehat{\Omega}| = 1 - |\Omega_p|/|\widehat{\Omega}|$, hence the porosity related to the pores volume is $\phi_p = 1 - c$.

2.3.1. Helmholtz resonators

The Helmholtz resonator Ω_H is made of a "chamber" domain $\widetilde{\Omega}$ and a constricted "duct" domain Ω'. The chamber is delimited by an impervious rigid surface $\widetilde{\Gamma}$ of negligible thickness. The duct Ω', of length $\ell' = O(\ell)$, constant section Σ, impervious wall Γ', connects the chamber to the "external" pores Ω_p. A morphological contrast is imposed by assuming that $|\Sigma|/\ell^2 \ll 1$. Thus, the volume of the duct $|\Omega'| = O(|\Sigma|\ell)$ can be disregarded compared to that of the chamber, $|\Omega'|/|\widetilde{\Omega}| = O(|\Sigma|/\ell^2) \ll 1$, and $|\widetilde{\Omega}| \approx |\Omega_H|$. For better compactness of the arrangement, the duct is located inside the chamber so that the interface between the pores and the resonator is $\Gamma = \widetilde{\Gamma} \cup \Sigma$. As an example, Fig. 3 depicts a resonator made of a spherical cavity and an internal duct.

Let us remind the "spring–mass" behavior of a Helmholtz resonator submitted to an external perturbation of pressure P. Since the chamber is much larger than the duct, the volume variation in the duct is negligible compared to that in the chamber. Thus, the motion u' of the gas mass $\rho^e|\Omega'|$ in the duct is reasonably assumed uniform and a volume $u'|\Sigma|$ is injected in the chamber. Hence, the resulting perturbation of pressure in the chamber reads (assuming here adiabatic compression): $\widetilde{P} = \gamma P^e u'|\Sigma|/|\widetilde{\Omega}|$. In addition, the motion $\widetilde{u}$ in the chamber is much smaller than the motion u' in the duct since $O(\widetilde{u}/\ell) = O(\widetilde{P}/\gamma P^e) = O(u'|\Sigma|/|\widetilde{\Omega}|)$ so that,

$$O(\widetilde{u}/u') = |\Sigma|/\ell^2 \ll 1.$$

Finally, the mass undergoes a force $\widetilde{P}|\Sigma|$, from which we deduce the equivalent spring of the gas chamber:

$$\mathrm{k} = \frac{\widetilde{P}|\Sigma|}{u'} = \frac{\gamma P^e |\Sigma|^2}{|\widetilde{\Omega}|}.$$

Disregarding the viscous effects, the momentum balance driving the mass in the duct submitted to P and $\widetilde{P}$ on its extremities reads:

$$-(\widetilde{P} - P)|\Sigma| = -\rho^e \omega^2 |\Omega'| u', \quad \text{i.e., } \mathrm{k}u' - \rho^e |\Omega'| \omega^2 u' = P|\Sigma|.$$

Consequently, the well known resonance frequency $f_0 = \omega_0/2\pi$ of the resonator reads:

$$\omega_0 = 2\pi f_0 = \sqrt{\frac{\mathrm{k}}{\rho^e|\Omega'|}} = \mathcal{C}^e\frac{|\Sigma|}{\sqrt{|\widetilde{\Omega}||\Omega'|}} = O\left(\frac{\mathcal{C}^e}{\ell}\frac{\sqrt{|\Sigma|}}{\ell}\right). \tag{11}$$

In the following sections, this leading physics is completed in order to take into account the thermal and viscous dissipations.

2.3.2. Conditions for co-dynamic regime

Consider first the case $\omega_0 > \omega_c$, i.e. the Helmholtz resonance ω_0 belongs to the frequency range of inertial regime in the pore network. Then the co-dynamic condition is naturally fulfilled. Indeed, in this case, according to ((10)–(11)) (disregarding for this estimate the possible change of macroscopic wavelength around resonance; but still, the conclusion can be a posteriori checked to be correct) and to the fact that $|\Sigma|/\ell^2 \ll 1$

$$\frac{\Lambda_p(\omega_0)}{2\pi} = O\left(\frac{\mathcal{C}^e}{\sqrt{\alpha_{p\infty}}\omega_0}\right) = \ell\frac{\ell}{\sqrt{|\Sigma|}} \gg \ell.$$

This inequality implies (i) that the resonance occurs at a frequency much lower than the diffraction frequency so that the scale separation assumption is satisfied, and (ii) ensures the coexistence of local dynamics (at the resonator scale) and global dynamics (at a scale much larger than the resonators). From the expressions of ω_0 and ω_c this situation arises for pores network permeability sufficiently large to have:

$$\frac{\mathcal{K}_p\alpha_{p_\infty}}{\ell\phi_p}\frac{\rho^e\mathcal{C}^e}{\mu} > O\left(\frac{\ell}{\sqrt{|\Sigma|}}\right) = O\left(\frac{1}{\sqrt{\varepsilon}}\right) > 1.$$

Now, if the resonance occurs within the viscous regime of the pore network, i.e. $\omega_0 < \omega_c$, then the co-dynamic condition is restrictive. Indeed, the scale separation condition $\Lambda_p(\omega_0)/(2\pi) \gg \ell$ reads in that case (see (10)):

$$\frac{\mathcal{K}_pP^e}{\omega_0\mu\phi_p} \gg \ell^2.$$

The specifications $\omega_0 < \omega_c$ and $\Lambda_p(\omega_0)/(2\pi) \gg \ell$ yield the following conditions for the permeability:

$$\sqrt{|\Sigma|}\frac{\alpha_{p_\infty}}{\gamma} \ll \frac{\mathcal{K}_p\alpha_{p_\infty}}{\phi_p}\frac{\rho^e\mathcal{C}^e}{\mu} < \frac{\ell^2}{\sqrt{|\Sigma|}}$$

that is rewritten, after dividing by ℓ and reminding that $\alpha_{p_\infty}/\gamma = O(1)$ and $\sqrt{|\Sigma|}/\ell = O(\sqrt{\varepsilon})$:

$$O\left(\sqrt{\varepsilon}\right) \ll \frac{\mathcal{K}_p\alpha_{p_\infty}}{\ell\phi_p}\frac{\rho^e\mathcal{C}^e}{\mu} < O\left(\frac{1}{\sqrt{\varepsilon}}\right).$$

This provides the necessary order of magnitude of the permeability to enables to reach the co-dynamic regime together with a viscous regime in the pore network.

$$\frac{\mathcal{K}_p\alpha_{p_\infty}}{\ell\phi_p}\frac{\rho^e\mathcal{C}^e}{\mu} = O(1).$$

To sum up, both situations show that co-dynamic situations occur only when a inertial or a visco-inertial regime prevail in the pore network. This imposes the following minimum value for the permeability

$$\frac{\mathcal{K}_p\alpha_{p_\infty}}{\phi_p} \geq \frac{\mu}{\rho^e\mathcal{C}^e}O(\ell) \quad \text{i.e.,} \omega_0/\omega_c \geq O\left(\frac{\sqrt{|\Sigma|}}{\ell}\right). \tag{12}$$

Conversely, if the pores network is too resistive, i.e. when the Helmholtz resonance should belong to the almost purely viscous regime ($\omega_0/\omega_c \ll 1$), then this "outside resistance" avoids the resonance phenomenon, and consequently the "co-dynamics" regime is not possible.

2.3.3. Problem at the local scale

In the pores, the duct and the chamber, the usual balance equations driving the perturbation of the pressure, of the temperature, the velocity and the heat flux are those given by the set (2)–(5). However, the boundary conditions and the rescaled equations and variables have to be specified to correctly reflect the specific regime that prevails in the different domains. The variables are indexed by $_p$ in the pores, denoted by a prime in the duct and by a tilde in the chamber.

In the pores Ω_p, the pressure, the temperature and the velocity are expanded as:

$$\begin{aligned} p_p(\mathbf{x},\mathbf{y}) &= p_p^{(0)}(\mathbf{x},\mathbf{y}) + \varepsilon p_p^{(1)}(\mathbf{x},\mathbf{y}) + \cdots \\ \theta_p(\mathbf{x},\mathbf{y}) &= \theta_p^{(0)}(\mathbf{x},\mathbf{y}) + \varepsilon\theta_p^{(1)}(\mathbf{x},\mathbf{y}) + \cdots \\ \mathbf{v}_p(\mathbf{x},\mathbf{y}) &= \mathbf{v}_p^{(0)}(\mathbf{x},\mathbf{y}) + \varepsilon\mathbf{v}_p^{(1)}(\mathbf{x},\mathbf{y}) + \cdots. \end{aligned} \tag{13}$$

The local physics is not modified by the resonators and the rescaling described in Eqs. (7)–(8) applies. The only modification concerns the boundary conditions (6) on Γ that have to be decomposed into conditions on the impervious surface $\widetilde{\Gamma}$ and on the small duct section Σ:

$$\mathbf{v}_p = \mathbf{0}, \qquad \theta_p = 0 \quad \text{on } \widetilde{\Gamma}; \qquad \mathbf{v}_p = \widetilde{\mathbf{v}}', \qquad p_p = p' \quad \text{on } \Sigma. \tag{14}$$

The geometrical contrast between $|\Sigma|$ and ℓ^2 is expressed mathematically by setting $|\Sigma| = O(\varepsilon\ell^2)$. This difference in magnitude is of first importance. Indeed, even if the velocity $\mathbf{v}'$ in the duct is of the same order as the velocity in the porous matrix, the flux $q_H = |\mathbf{q}_H|$ pulsed by the resonator at its aperture is of one order smaller than the flux $q_p = |\mathbf{q}_p|$ carried through the pores, indeed $O(q_H/q_p) = O(\|\mathbf{v}'\|\Sigma|/|\mathbf{v}_p|\ell^2) = O(|\Sigma|/\ell^2) \ll 1$. The fact that $O(q_H/q_p) \leq O(\varepsilon)$ is consistent with the scale separation assumption. Indeed, under long wavelength, the mean flux presents small variations $O(\varepsilon q_p)$ between the two extremities of the cell. By mass conservation, these variations include the flux pulsed by the resonator, that consequently must be of one order smaller than q_p, i.e. $q_H = O(\varepsilon q_p)$.

In the duct Ω', the pressure p', the temperature θ' and the velocity $\mathbf{v}'$ are of the same order as in the pores and are expanded as in (13). Furthermore, we have seen (see 2.3.1) that the pressure varies at the *local* scale (as the shear stresses). Consequently, when using the $(\mathbf{x}, \mathbf{y})$ variables, the terms $\mu\mathbf{div}(\mathbf{D}(\mathbf{v}'))$ and $\nabla p'$ have to be rescaled as $\mu(\ell/L)^2\mathbf{div}(\mathbf{D}(\mathbf{v}')) = \mu\varepsilon^2\mathbf{div}(\mathbf{D}(\mathbf{v}'))$ and $\ell/L\nabla p' = \varepsilon\nabla p'$. Thus, the "$x$–$y$-rescaled" Navier–Stokes and Fourier equations take the following form in the duct:

$$\mu\varepsilon^2\mathbf{div}(\mathbf{D}(\mathbf{v}')) - \varepsilon\nabla p' = i\omega\rho^e\mathbf{v}' \quad \text{on } \Omega'. \tag{15}$$

The boundary conditions read:

$$\mathbf{v}' = 0, \qquad \theta' = 0 \quad \text{on } \Gamma'; \qquad \mathbf{v}' = \widetilde{\mathbf{v}}, \qquad p' = \widetilde{p} \quad \text{on } \widetilde{\Sigma}. \tag{16}$$

For exhaustiveness, the rescaled Fourier equation reads $\varepsilon^2\mathrm{div}(\kappa\nabla\theta') - i\omega(\rho^e c_p\theta' - p')$ but this equation is not involved in the leading order resolution, and is not considered for further developments.

In the chamber $\widetilde{\Omega}$, the pressure $\widetilde{p}$ and the temperature $\widetilde{\theta}$ are of the same order as in the pores but the velocity $\widetilde{\mathbf{v}}$, is of one order smaller (since $O(\widetilde{u}/u') = |\Sigma|/\ell^2 = O(\varepsilon)$ see previous section). Hence, the velocity is here expanded in the form:

$$\widetilde{\mathbf{v}}(\mathbf{x}, \mathbf{y}) = \varepsilon\widetilde{\mathbf{v}}^{(1)}(\mathbf{x}, \mathbf{y}) + \cdots. \tag{17}$$

In the chamber, the pressure is quasi-uniform while the shear stresses vary at the local scale. Consequently, the terms $\mu\mathbf{div}(\mathbf{D}(\widetilde{\mathbf{v}}))$ and $\mathrm{div}(\kappa\nabla\widetilde{\theta})$ are rescaled as $\mu\varepsilon^2\mathbf{div}(\mathbf{D}(\widetilde{\mathbf{v}}))$ and $\varepsilon^2\mathrm{div}(\kappa\nabla\widetilde{\theta})$. Hence, the "$x$–$y$-rescaled" Navier–Stokes and Fourier equations together with the boundary conditions are:

$$\mu\varepsilon^2\mathbf{div}(\mathbf{D}(\widetilde{\mathbf{v}})) - \nabla\widetilde{p} - i\omega\rho^e\widetilde{\mathbf{v}} = \mathbf{0} \quad \text{on } \widetilde{\Omega} \tag{18}$$

$$\varepsilon^2\mathrm{div}(\kappa\nabla\widetilde{\theta}) - i\omega(\rho^e c_p\widetilde{\theta} - \widetilde{p}) = 0 \quad \text{on } \widetilde{\Omega} \tag{19}$$

$$\widetilde{\mathbf{v}} = \mathbf{0}, \qquad \widetilde{\theta} = 0 \quad \text{on } \Gamma'. \tag{20}$$

Remark. The boundary conditions between the pores, duct and chamber are expressed on the sections of the duct at its extremities Σ and $\widetilde{\Sigma}$. Other shapes of virtual surfaces delimiting the duct – for instance hemispheric boundaries – could have been chosen, provided that their surface remain of the same order as the duct section. Hence, since $\Sigma = O(\varepsilon)\ell^2$, this relative arbitrariness modifies the determination of the microscopic response fields at the ε-order only, cf. [11], and then can be disregarded for a leading order description. Besides, the modeling could be improved by introducing matched asymptotics to address the field transitions between the different domains.

2.3.4. Main steps of the up-scaling

The homogenization process applied to this local description can be summarized as follows. As for impervious grains, the pore pressure varies at the macroscale i.e. $p_p^{(0)}(\mathbf{x}, \mathbf{y}) = P^{(0)}(\mathbf{x})$. Then, at the next order, since the flux $q_H^{(1)}$ induced by the resonators is of one order smaller than that in the pores $q_p^{(0)}$, the dynamic flow around the resonators under the forced macroscopic pressure gradient is, at the leading order, the same as if the Helmholtz resonator were impervious. For the same reason the heat flux imposed by the resonator is negligible at the leading order. *Thus, we are left with the usual derivation of the dynamic permeability and the effective compressibility, with identical problems as that encountered with impervious grains.* Consequently the dynamic Darcy's law and the effective compressibility of the gas in the pores take the classic forms. The next step consists in establishing the mass balance of the whole period. At this order, the mass flux $q_H^{(1)}$ due to the resonators appears as an additional source term that does not exist in the conventional situation where the grains are impervious.

This source term is determined by the resolution in the resonators: at the leading order the pressure $\widetilde{P}^{(0)}$ in the chamber is shown to be uniform, and is related to the flux $q_H^{(1)}$ through the mass balance in the whole chamber

$$-q_H^{(1)} + i\omega\widetilde{P}^{(0)}\frac{1 - \widetilde{\Pi}(\omega)}{P^e}|\widetilde{\Omega}| = 0. \tag{21}$$

In this expression, $\widetilde{\Pi}(\omega)$ is the "thermal function" of the chamber that accounts for the non uniform density due to heat transfer in the gas in contact with the isothermal solid interface Γ. $\widetilde{\Pi}(\omega)$ presents the same properties as $\Pi_p(\omega)$, i.e. $1-\widetilde{\Pi} \to 1$ at low frequency and $1-\widetilde{\Pi} \to 1/\gamma$ at high frequency. In the meantime, the flow in the duct is driven by the pressure difference $\widetilde{P}^{(0)} - P^{(0)}$ between its two extremities and the velocity can be expressed in the form:

$$\mathbf{v}'^{(0)}(\mathbf{x},\mathbf{y}) = -\frac{\boldsymbol{\zeta}(\omega,\mathbf{y})}{i\omega\rho^e}\frac{\widetilde{P}^{(0)} - P^{(0)}}{\ell'}.$$

Consequently, the mean flux $q_H^{(1)}$ reads:

$$q_H^{(1)} = \int_\Sigma \mathbf{v}'^{(0)}.\mathbf{n}ds = -\frac{|\Sigma|}{i\omega\rho^e\tau'(\omega)}\frac{\widetilde{P}^{(0)} - P^{(0)}}{\ell'} \tag{22}$$

where $\tau'(\omega)$ is the dynamic tortuosity of the duct defined by:

$$\tau'(\omega) = \left[\frac{1}{|\Sigma|}\int_\Sigma \boldsymbol{\zeta}(\omega,\mathbf{y}).\mathbf{n}ds\right]^{-1}.$$

Finally, equating expressions (21) and (22), eliminating $\widetilde{P}^{(0)}$, and assuming straight ducts (i.e. $|\Omega'| = |\Sigma|\ell'$), the flux $q_H^{(1)}$ due to the resonators is related to the pores pressure $P^{(0)}$ through the resonator transfer function, namely

$$q_H^{(1)} = i\omega\frac{P^{(0)}}{P^e}\frac{1-\widetilde{\Pi}(\omega)}{1-(\omega/\omega_0)^2\tau'(\omega)}|\widetilde{\Omega}|.$$

2.3.5. Unconventional poro-acoustics

Finally, at the leading order, the driving set of equations for a concentration c of resonators (and an inter-resonator porosity $\phi_p = 1-c$) reads where $\mathbf{V}$ is the integral of the velocity in the pores, divided by the total cell volume and P is the pore pressure:

$$\mathrm{div}(\mathbf{V}) + i\omega\frac{P}{P^e}\left((1-c)(1-\Pi_p(\omega)) + c\frac{1-\widetilde{\Pi}(\omega)}{1-(\omega/\omega_0)^2\tau'(\omega)}\right) = 0 \tag{23}$$

$$\mathbf{V} = -\frac{K_p(\omega)}{\mu}\nabla P. \tag{24}$$

This set constitutes the macroscopic description, where the involved variables and derivative are all defined according to the macroscopic space variable, and the macroscopic parameters are deduced from the knowledge of the microstructure. As the flux pulsed by the resonator is one order smaller than the flux in the pores, the dynamic permeability and the effective compressibility of the gas *in the pores* are identical as those corresponding to impervious grains. This formulation accounts for the co-dynamic regime in the media, with the simultaneous occurrence of macroscopic wavelength and local dynamics in the resonator.

Two distinct pressure fields are present at the period scale, $P = P^{(0)}$ that "carries" the macroscopic wave, and $\widetilde{P}^{(0)}$ developed in the resonator as forced response to $P^{(0)}$. Conversely to conventional media, and as already observed in double porosity media [7], the governing macroscopic variable P is not the mean pressure in the whole gas volume, but the pressure in the pore volume only. Note however, that as in conventional media, the macroscopic Poynting vector $P\mathbf{V}$ at the leading order is the mean of the local Poynting vector $p\mathbf{v}$. Indeed

$$\int_{\Omega_p\cup\Omega_h} p\mathbf{v}d\Omega = \int_{\Omega_p} p_p\mathbf{v}_p d\Omega + \int_{\widetilde{\Omega}} \widetilde{p}\widetilde{\mathbf{v}}d\Omega + \int_{\Omega'} p'\mathbf{v}'d\Omega$$

and since (i) the flux $\widetilde{\mathbf{v}}$ is of one order smaller in the chamber than in the pores and (ii) the duct volume Ω' is of one order smaller than the cell volume, we have:

$$\left[\frac{1}{\widetilde{\Omega}}\int_{\Omega_p\cup\Omega_h} p\mathbf{v}d\Omega\right]^{(0)} = \frac{1}{\widetilde{\Omega}}\int_{\Omega_p} P^{(0)}\mathbf{v}^{(0)}d\Omega = P\frac{1}{\widetilde{\Omega}}\int_{\Omega_p}\mathbf{v}^{(0)}d\Omega = P\mathbf{V}.$$

These two observations are consistent with the non local theory developed in [12] and it is easy to check that they apply systematically in the different non-conventional models presented in the sequel.

The comparison with the conventional poro-acoustic shows that the resonators does not modify the effective dynamic permeability while the effective bulk modulus is significantly changed as detailed here-below and shown later experimentally.

The key effect of the resonator lies in the unconventional effective bulk modulus $E(\omega)$ of the gas that reads:

$$E(\omega) = P^e\left((1-c)(1-\Pi_p(\omega)) + c\frac{1-\widetilde{\Pi}(\omega)}{1-(\omega/\omega_0)^2\tau'(\omega)}\right)^{-1} \tag{25}$$

or equivalently:

$$E(\omega)=\left(\frac{1-c}{E_p}+\frac{c}{E_H}\right)^{-1};\qquad E_p(\omega)=\frac{P^e}{1-\Pi_p(\omega)};\qquad E_H(\omega)=P^e\frac{1-(\omega/\omega_0)^2\tau'(\omega)}{1-\widetilde{\Pi}(\omega)}.$$

The geometric mean involved in this formulation discloses an association *in series* of (i) the effective gas stiffness in the pores E_p and of (ii) the apparent stiffness E_H of the resonator, each being weighted by the volume ratio of its respective domain. The atypical feature is clearly evidenced when disregarding the viscous dissipation effects and considering adiabatic regime so that:

$$E(\omega)\approx E_{adiab}(\omega)=\gamma P^e\left((1-c)+\frac{c}{1-(\omega/\omega_0)^2}\right)^{-1}$$

meaning that the apparent stiffness associated to the resonator is negative for $\omega>\omega_0$, and, in turn, the effective bulk modulus is negative in the "atypical band" $[\omega_0,\omega_0^*]$, where

$$\omega_0^*=\omega_0\sqrt{1+\frac{c}{1-c}}\quad\text{and}\quad E_{adiab}(\omega_0)=0;\qquad E_{adiab}(\omega_0^{*\pm})=\pm\infty.$$

Even if the dissipation tends to regularize the behavior (absolute values are never zero nor infinite), a strong effect of the resonator remains and drastic changes in the global behavior occurs as observed experimentally and numerically in Section 4.

2.4. Porous media with embedded resonators

In this section, the resonator packing is identical as in the previous section, but the interspace is now occupied by a rigid porous matrix of porosity ϕ_m. Hence, the period $\widehat{\Omega}$ contains the porous matrix domain Ω_m and the resonator Ω_H. The concentration of resonators is $c=|\Omega_H|/|\widehat{\Omega}|=1-|\Omega_m|/|\widehat{\Omega}|$. The pores of the matrix are assumed much smaller than ℓ. Thus, at the period scale, the matrix is regarded as an equivalent homogeneous medium, described by the usual poro-acoustics. For a detailed analysis of this situation the reader can refer to [11].

2.4.1. Formulation of the problem at the local scale

In the porous matrix Ω_m, the governing equations are that of a conventional porous medium, as given in Section 2.2.2, except that the variables and parameters are now indexed by $_m$. For simplicity, the matrix is assumed isotropic and the dynamic permeability tensor and dynamic tortuosity tensor reduce to the scalar functions K_m and $\tau_m=\mu\phi_m/(i\omega\rho^e\mathcal{K}_m)$. Now, the mean velocity varies at the period scale in order to match the boundary conditions on the interface Γ with the resonator. These latter are impervious condition on $\widetilde{\Gamma}$ and continuity of flux and pressure on the small surface Σ. Thus, the description in the porous matrix Ω_m reads, where $\mathbf{v}_m$, is the Darcy velocity, i.e. the mean velocity in the pores of the matrix, times the matrix porosity ϕ_m:

$$\operatorname{div}(\mathbf{v}_m)+i\omega\frac{p}{P^e}\phi_m(1-\Pi_m)=0 \tag{26}$$

$$\mathbf{v}_m=-\frac{K_m}{\mu}\cdot\nabla p_m \tag{27}$$

$$\mathbf{v}_m\cdot\mathbf{n}=0\quad\text{on }\widetilde{\Gamma};\qquad \mathbf{v}_m\cdot\mathbf{n}=\mathbf{v}'\cdot\mathbf{n},\qquad p_m=p'\quad\text{on }\Sigma \tag{28}$$

$$\mathbf{v}_m,\ p_m,\ \widehat{\Omega}\text{-periodic}. \tag{29}$$

Because of the scale separation, the pressure and volume variation vary at the macroscale (i.e. long wavelength scale). Consequently, these equations do not need to be rescaled when re-expressed with the double $(\mathbf{x},\mathbf{y})$ variable system, since L is the reference length. As in the previous case, the fact that $|\Sigma|=O(\varepsilon\ell^2)=O(\varepsilon|\Gamma|)$, imposes that the flux pulsed by the resonator is one order smaller than the flux carried through the matrix. Hence, the relative order of magnitude in the different domains are preserved and the variables p_m and $\mathbf{v}_m$ in the porous matrix are expanded as in (13).

In the Helmholtz resonator Ω_H, the local description is identical to that given in Section 2.3.3.

2.4.2. Overview of the up-scaling process

Accordingly with the scale separation, one first shows that the pore pressure varies at the macroscopic scale, i.e. $p_m^{(0)}(\mathbf{x},\mathbf{y})=P^{(0)}(\mathbf{x})$. Then, as the flux induced by the resonators is of one order smaller than that of the pores, it is not involved in the determination of the flux at the leading order. Hence, one obtains a periodic local problem of conduction, where the matrix is characterized by its dynamic permeability and the resonators appear as impervious. This leads to a macroscopic dynamic Darcy's law, where the effective permeability is that of the matrix corrected by a real and dimensionless "shape" tensor. This latter tensor is nothing but the inverse of the tortuosity tensor of the matrix domain, see [11], and reduces to a scalar $A_m<1$ in the case of macroscopic isotropy. The next step consists in deriving the mass balance. The flux due to the resonators appears as an additional source term (determined as in absence of the porous matrix) that adds up with the conventional compressibility term due the porous matrix.

2.4.3. Macroscopic description

In summary, at the leading order, and in the isotropic case, the macroscopic description is given by the set of equations (remind that $1-c=|\Omega|_H/|\widehat{\Omega}|$), valid up to a precision ε:

$$\mathrm{div}(\mathbf{V})+i\omega\frac{P}{P^e}\left((1-c)\phi_m(1-\Pi_m(\omega))+c\frac{1-\widetilde{\Pi}(\omega)}{1-(\omega/\omega_0)^2\tau'(\omega)}\right)=0 \tag{30}$$

$$\mathbf{V}=-\frac{A_mK_m(\omega)}{\mu}\nabla P. \tag{31}$$

Here $\mathbf{V}$ is the integral of the velocity in the matrix domain, divided by the total cell volume and P is the pressure in the matrix. This description is very similar to that established in absence of porous matrix. The only difference lies in the effective permeability and in the contribution to the effective bulk modulus inherited from the matrix. The same qualitative comments on the particular feature of such media still applies. From classic results on conduction in heterogeneous media [21], or on tortuosity [22], we necessarily have $A_m<1-c$, i.e, the effective permeability is reduced compared to that of the matrix. Further, for resonators in a concentration $c\leq 1/3$, A_m can be assessed accurately by $A_m\approx 2(1-c)/(2+c)$.

2.5. Several possible extensions

Several other morphological options can lead to inner resonance. Whatever the case, the resonator design should be such that the resonating effect induces a small flux (on average on the period) compared to the macroscopic flux.

2.5.1. Multiple inner resonators

Instead of having a single type of oscillator, the period may contains several different oscillators, or additional impervious inclusions (of the same magnitude as the size of the resonator). For instance:

- if the medium is made of two types of Helmholtz resonators (indexed by 1, 2, in concentration c_1 and c_2, $c_1+c_2=c$), the mass balance (30) will be replaced by

$$\mathrm{div}(\mathbf{V})+i\omega\frac{P}{P^e}\left((1-c)(1-\Pi_p(\omega))+c_1\frac{1-\widetilde{\Pi}_1(\omega)}{1-(\omega/\omega_{01})^2\tau_1'(\omega)}+c_2\frac{1-\widetilde{\Pi}_2(\omega)}{1-(\omega/\omega_{02})^2\tau_2'(\omega)}\right)=0$$

- if the medium is made of a single type of Helmholtz resonator in concentration $c_H=|\Omega_H|/|\widehat{\Omega}|$ and impervious grains in concentration $c_g=|\Omega_g|/|\widehat{\Omega}|$, the porosity related to the pores is now $\phi_p=1-(c_H+c_g)$ and the mass balance (30) becomes

$$\mathrm{div}(\mathbf{V})+i\omega\frac{P}{P^e}\left((1-(c_H+c_g))(1-\Pi_p(\omega))+c_H\frac{1-\widetilde{\Pi}(\omega)}{1-(\omega/\omega_0)^2\tau'(\omega)}\right)=0.$$

More generally, if we have in a period (with or without porous matrix) N resonators (indexed by i) tuned at different frequencies, the effective bulk modulus becomes:

$$E(\omega)=\left(\frac{1-\phi_p}{E_p}+\sum_{i=1}^{N}\frac{c_i}{E_i}\right)^{-1} \tag{32}$$

where E_p is the apparent bulk modulus of the inter-resonator pore space (of porosity $\phi_p=1-\sum_{i=1}^{N}c_i$), and E_i the apparent bulk modulus of the each type of resonator ($E=\infty$ for impervious grains). In all these cases, the dynamic permeability at the leading order, see (24), will be the same as if all "grains" were impervious. In these different configurations, the global effect is expected to be visible on frequency bands of influence of each resonator considered independently.

2.5.2. Other type of resonators

The geometry can be changed to enhance the dissipation. For example, the single straight duct Γ' can be replaced by several straight ducts of smaller diameters but identical lengths. This will change the apparent duct dynamic tortuosity $\tau'(\omega)$ and increase the viscous dissipation with (almost) no change in the fundamental eigen frequency of the resonator. Higher dissipation could also be achieved by filling the duct with porous media. For a straight duct, this results in replacing $\tau'(\omega)$ by $\tau'^*(\omega)/\phi'$ where $\tau'^*(\omega)$ and ϕ' are the dynamic tortuosity and porosity of the media filling the duct. Instead of the "spring–mass" resonance of Helmholtz resonators, one may also consider quarter wavelength resonators. In a frequency range such that the length of the resonating tube $\mathcal{L}_r$ matches the quarter wavelength of the acoustic wave, a resonance occurs. Nevertheless, to ensure the scale separation necessary for the co-dynamic regime, the size of the resonating domain should be much smaller than the wavelength. This implies to rearrange the tube in a compact domain Ω_r of characteristic size ℓ, for instance by wrapping the tube (see Fig. 4). As a consequence the tube section $\sigma=\Omega_r/\mathcal{L}_r$ should be of one order smaller than the period size, i.e. $\sigma=O(\ell^3/\Lambda)=O(\varepsilon\ell^2)$, which corresponds to the scaling of the Helmholtz resonator aperture.

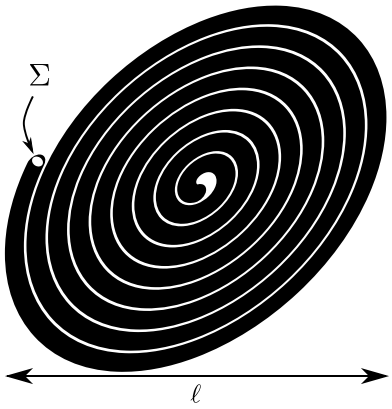

Fig. 4. Illustration 2D of wrapped quarter wavelength resonator enabling the scale separation of phenomena.

Disregarding the slight dissipation effects and the curved geometry, the pulsed flux of this device is that of a straight tube:

$$q_r^{(1)} = iP^{(0)}\frac{\sigma}{\rho^e \mathcal{C}^e}\tan\left(\frac{\pi}{2}\frac{\omega}{\omega_{0r}}\right) \quad \text{with } \omega_{0r} = \frac{\pi}{2}\frac{\mathcal{C}^e}{\mathcal{L}_r}.$$

Then the mass balance of this arrangement of compacted quarter wavelength resonators, in concentration $c = |\Omega_r|/|\widehat{\Omega}|$, reads:

$$\operatorname{div}(\mathbf{V}) + i\omega\frac{P}{P^e}\left((1-c)(1-\Pi_p(\omega)) + \frac{c}{\gamma}\frac{2}{\pi}\frac{\omega_{0r}}{\omega}\tan\left(\frac{\pi}{2}\frac{\omega}{\omega_{0r}}\right)\right) = 0.$$

Similarly to the "spring–mass" behavior, we observe that the effective bulk modulus may be negative in frequency range(s) close to the inner resonance(s). Indeed, considering adiabatic regime, in the vicinity of ω_{0r} the bulk modulus of the medium can be approximated by:

$$\gamma P^e\left[1 - c + \frac{2}{\pi}\frac{c}{1-\omega/\omega_{0r}}\right]^{-1}.$$

Consequently, the atypical band of a negative effective modulus is $[\omega_{0r}, \omega_{0r}^*]$, where

$$\omega_{0r}^* = \omega_{0r}\left(1 + \frac{2c}{\pi(1-c)}\right). \tag{33}$$

This description also applies to media with "dead-end pores" [23] provided that the above geometrical requirements are fulfilled.

Besides elasto-inertial resonance with weak dissipation one may also consider "visco-inertial resonance". An example is the double porosity media [7,8,24], that can be realized by replacing impervious grains by microporous grains (of volume Ω_μ, boundary Γ_μ and internal porosity ϕ_μ) having an intrinsic permeability $\mathcal{K}_\mu$ much smaller than that of the interstitial pore network. In this case, a dynamic regime of pressure diffusion arises, governed by the gas compressibility, the micro-permeability of the grains and their size. Here again the dynamic effective permeability is kept unchanged, but the mass balance is replaced by:

$$\operatorname{div}(\mathbf{V}) + i\omega\frac{P}{P^e}\left((1-c)(1-\Pi_p(\omega)) + c\phi_\mu F_d\left(\frac{\omega}{\omega_d}\right)\right) = 0.$$

As mentioned in [7], the characteristic diffusion frequency ω_d and the function F_d can be approximated under the generic form (see [25]) where $L_d = \Omega_\mu/\Gamma_\mu$ and M is a geometric form factor $O(1)$:

$$\omega_d = \frac{P^e\mathcal{K}_g}{\mu\phi_\mu L_d^2}; \qquad F_d(x) = 1 - \frac{ix}{ix + \sqrt{1 + ixM/2}}.$$

Conversely to elasto-inertial case, the visco-inertial diffusion function does not exhibit any poles in the real frequency axis. Consequently, in the vicinity of the diffusion frequency ω_d, the effective bulk modulus is mostly changed in its imaginary part and no atypical band of negative effective bulk modulus appear.

2.5.3. Non periodic distribution

The assumption of periodicity is not a strict requirement for the distribution of resonators. Indeed, when a separation of scales exists, i.e. for long wavelengths, periodic materials and non-periodic materials with ERV show macroscopic behavior of the same nature [15]. Therefore, a similar homogenized description applies if the resonators are non-periodically distributed. However, the local solution is not reducible to a well-defined problem on a periodic cell and may only be solved numerically.

2.6. Features of conventional and non-conventional wave propagation

2.6.1. Generic formulation and acoustic wave parameters

Both conventional and unconventional models can be formulated in the generic form:

$$\begin{aligned} &\mathrm{div}(\mathbf{V}) + i\omega \frac{P}{E(\omega)} = 0 \\ &\mathbf{V} = -\frac{K(\omega)}{\mu}\nabla P = -\frac{1}{i\omega D(\omega)}\nabla P. \end{aligned} \tag{34}$$

The difference between the models lies in the specific form taken by the effective bulk modulus $E(\omega)$, dynamic permeability $K(\omega)$ (or apparent density $D(\omega)$). Eliminating the flux $\mathbf{V}$ gives the wave equation:

$$E(\omega)\Delta P + \omega^2 D(\omega) P = 0. \tag{35}$$

Considering an harmonic plane wave $P = P_0 \exp[i(\omega t - k(\omega)x)]$, we deduce the complex and frequency dependent wave number $k(\omega)$ and wave velocity $\mathcal{C}(\omega) = \frac{\omega}{k(\omega)}$. The dimensionless wave number k^* and wave velocity $\mathcal{C}^*$ normalized by the air characteristics are

$$\mathcal{C}^*(\omega) = \frac{\mathcal{C}(\omega)}{\mathcal{C}_{air}} = \frac{k_{air}}{k^*(\omega)} = \sqrt{\frac{E(\omega)}{D(\omega)}\frac{\rho^e}{\gamma P^e}}.$$

The characteristic impedance Z of the medium and its dimensionless value Z^* normalized by the air impedance Z_{air} are respectively defined as

$$Z(\omega) = \frac{P}{V} = R(\omega)\mathcal{C}(\omega) = \sqrt{E(\omega)D(\omega)}; \qquad Z^*(\omega) = \frac{Z(\omega)}{Z_{air}} = \sqrt{\frac{E(\omega)D(\omega)}{\gamma P^e \rho^e}}.$$

At the interface between two media one defines the surface impedance as $Z_s = P/V|_{interface}$. For waves of normal incidence, in the usual situation where the medium is a plane layer of thickness d in contact with a rigid impervious wall, a standard calculus yields

$$Z_s = -iZ(\omega)\cot(k(\omega)d).$$

Now for a plane wave propagating in air at normal incidence, the ratio of the reflected to incident pressure amplitude is given by the reflection coefficient, classically expressed as:

$$R(\omega) = \frac{Z_s - Z_{air}}{Z_s + Z_{air}} = \frac{-iZ^*\cot(kd) - 1}{-iZ^*\cot(kd) + 1}$$

and the absorption coefficient at normal incidence, that assesses the energy absorbed compared to the incident energy reads:

$$A(\omega) = 1 - |R|^2 = \frac{2\mathrm{Im}(Z^*\cot(kd))}{|-iZ^*\cot(kd) + 1|^2}; \quad 0 \le A(\omega) \le 1.$$

For non-dissipative materials the wave number and impedance are real, $|R| = 1$, and the absorption is null. For weakly dissipative materials, the characteristic impedance presents a weak imaginary and varies slowly with the frequency. Then, the frequency variation of the absorption are mainly governed by the term $\cot(kd)$, and the frequency range of maximum of A occurs around the minimum of $|-iZ^*\cot(kd) + 1|^2$. Because of the weak imaginary parts, the first minimum of this latter occurs in the vicinity of $\mathrm{Re}(k)d = \pi/2$. Hence, the maximum of absorption (of weak value) is expected in a frequency range close to the quarter wavelength resonance. Conversely, for highly dissipative (and dispersive) materials, the absorption may be close to 1, in the frequency range where $Z^*\cot(kd)$ is close to i.

2.6.2. Reference case: conventional porous media

The above expressions applied to a conventional porous medium, give the dimensionless sound velocity $\mathcal{C}_c^*(\omega)$:

$$\mathcal{C}_c^*(\omega) = \sqrt{\frac{1}{\tau_p\gamma\,(1-\Pi_p)}} = \sqrt{\frac{i\omega K_p}{\rho^e\mu\phi_p\gamma\,(1-\Pi_p)}}.$$

At low frequencies, the flow is governed by the viscosity then, $K_p \to \mathcal{K}_p$, the real-valued intrinsic permeability ; and the perturbation is quasi-isotherm i.e. $1 - \Pi_p \to 1$. The acoustic waves tends to damped diffusive waves:

$$\mathcal{C}_c^*(\omega) \to \sqrt{\frac{i\omega\mathcal{K}_p}{\rho^e\mu\phi_p\gamma}}; \qquad \frac{\mathrm{Im}(\mathcal{C}_c^*)}{\mathrm{Re}(\mathcal{C}_c^*)} = \tan(\mathrm{Arg}(\mathcal{C}_c^*)) \to 1.$$

At high frequencies, the flow is governed by the inertia then the dynamic tortuosity tends to its real high frequency limit $\tau_p \to \alpha_{p_\infty}$; and the perturbation is quasi-adiabatic thus $1-\Pi_p \to 1/\gamma$. The waves tends to weakly damped elastic waves:

$$\mathcal{C}_c^*(\omega) \to \frac{1}{\sqrt{\alpha_{p_\infty}}}; \qquad \frac{\mathrm{Im}(\mathcal{C}_c^*)}{\mathrm{Re}(\mathcal{C}_c^*)} = \tan(\mathrm{Arg}(\mathcal{C}_c^*)) \to 0.$$

2.6.3. Inner resonance porous media: atypical dispersion and band gaps

The specificity of inner resonance media lies in the fact that, in absence of dissipation, the effective bulk modulus vanishes at the resonator eigen frequency ω_0, presents a singularity (pole) at ω_0^* and takes on negative values in the atypical frequency band $[\omega_0, \omega_0^*]$. This induces unusual properties that require a particular attention. For media made of resonators, (respectively made of resonators embedded in a porous matrix) the dimensionless sound velocity $\mathcal{C}_H^*(\omega)$ (resp. $\mathcal{C}_m^*(\omega)$) is expressed as:

$$\mathcal{C}_H^*(\omega) = \sqrt{\frac{1-c}{\tau_p(\omega)\gamma}\left((1-c)[1-\Pi_p(\omega)] + c\frac{1-\widetilde{\Pi}(\omega)}{1-(\omega/\omega_0)^2\tau'(\omega)}\right)^{-1}}$$

$$\mathcal{C}_m^*(\omega) = \sqrt{\frac{A\phi_m}{\tau_m(\omega)\gamma}\left((1-c)\phi_m[1-\Pi_m(\omega)] + c\frac{1-\widetilde{\Pi}(\omega)}{1-(\omega/\omega_0)^2\tau'(\omega)}\right)^{-1}}.$$

Because of the similarity of both expressions, we focus in the sequel on the media made of resonators. However similar conclusions may be drawn for resonators in a porous matrix, see [11]. Far from the resonance, $\mathcal{C}_H^*(\omega)$ presents the behavior of conventional media. The parameters of these conventional media will however not be the same in the LF and HF limits, indeed:

$$\text{when } \omega/\omega_0 \ll 1, \qquad \mathcal{C}_H^*(\omega) \approx \sqrt{\frac{1}{\tau_p(\omega)\gamma}\frac{1-c}{(1-c)[1-\Pi_p(\omega)] + c[1-\widetilde{\Pi}(\omega)]}} \tag{36}$$

$$\text{when } \omega/\omega_0 \gg 1, \qquad \mathcal{C}_H^*(\omega) \approx \sqrt{\frac{1}{\tau_p(\omega)\gamma}\frac{1}{(1-\Pi_p(\omega))}} \tag{37}$$

which indicates that at frequency lower than the resonance, the whole gas of the chamber participate to the effective stiffness, while at frequencies higher than the resonance, the behavior is the same as if the resonators were impervious.

Now, around the atypical frequency band, it is convenient to rewrite $\mathcal{C}_H^*(\omega)$ in the form:

$$\mathcal{C}_H^*(\omega) = \frac{\mathcal{C}_c^*(\omega)}{\sqrt{1+\frac{c}{1-c}\frac{1-\widetilde{\Pi}(\omega)}{1-\Pi_p(\omega)}\frac{1}{1-(\omega/\omega_0)^2\tau'(\omega)}}}$$

where the term under the root is the corrector factor compared to the conventional porous media, i.e. corresponding to impervious resonators. An exact analysis of this factor is difficult because of the complex values of the thermal functions. However, as the size of the pores and of the resonators are of the same order, the ratio $\frac{1-\widetilde{\Pi}(\omega)}{1-\Pi_p(\omega)}$ is in practice very close to 1. Moreover, setting this ratio to 1 would be exact in adiabatic regime where the thermal exchanges are negligible, i.e. $1-\Pi \approx 1/\gamma$. Thus the main features can be evidenced on the 'approximated' velocity indexed by ^{a} that takes the form:

$$\mathcal{C}_H^{*a}(\omega) = \mathcal{C}_c^*(\omega)\sqrt{\left(1+\frac{c}{1-c}\frac{1}{1-(\omega/\omega_0)^2\tau'(\omega)}\right)^{-1}}.$$

For frequency out of the atypical band, i.e. $\omega \notin [\omega_0, \omega_0^*]$, if the resonator dissipation is negligible, $\tau'(\omega) \approx 1$, the effective stiffness is real positive, and we simply have:

$$\mathcal{C}_H^{*a}(\omega) \approx \mathcal{C}_c^*(\omega)\sqrt{\left(1+\frac{c}{1-c}\frac{1}{1-(\omega/\omega_0)^2}\right)^{-1}}; \qquad Arg(\mathcal{C}_H^{*a}) \approx Arg(\mathcal{C}_c^*).$$

The nature of the waves (more or less attenuated or oscillating) defined by $Arg(\mathcal{C}(\omega))$ is (quasi)-identical to that of the conventional poro-acoustic waves that would exist if the resonators were impervious. However, in comparison with impervious grains, the effect of resonators is to decrease (resp. increase) the velocity and the wavelength for $0 \le \omega \le \omega_0$ (resp. $\omega \ge \omega_0^*$). This induces a large dispersion of the velocity as evidenced by the approximated values, $\mathcal{C}_H^{*a}(\omega_0) = 0$ and $|\mathcal{C}_H^{*a}(\omega_0^{*\pm})| = \infty$. In reality, these singular values and/or abrupt variations at ω_0 and ω_0^* are regularized by the weak dissipation brought by the resonator. This will be evidenced by the simulations and the experiments presented in Section 3.

For frequency in the atypical band, i.e. $\omega \notin [\omega_0, \omega_0^*]$, considering undamped resonators (taking $\tau'(\omega) = 1$) the effective bulk modulus takes on real negative values. Thus

$$\mathcal{C}_H^{*a}(\omega) \approx i\mathcal{C}_c^*(\omega)\sqrt{\left|1+\frac{c}{1-c}\frac{1}{1-(\omega/\omega_0)^2}\right|^{-1}}; \qquad Arg(\mathcal{C}_H^{*a}) \approx Arg(\mathcal{C}_c^*) + \pi/2.$$

The $\pi/2$-jump of $Arg(\mathcal{C}_H^{*a})$ in the atypical band modifies drastically the nature of the wave. Indeed, as $0 \leq Arg(\mathcal{C}_c^*) \leq \pi/4$ then $\pi/2 \leq Arg(\mathcal{C}_H^{*a}) \leq 5\pi/4$. Consequently the wave is over-damped and confined in boundary layers of characteristic size $\Lambda = |C_c(\omega)|(2\pi/\omega)$. This means that the atypical band is in fact a band gap of the media.

The differences of velocity between conventional and unconventional media are transferred on the characteristic impedances, since, as $K_H = K_c$,

$$\frac{Z_H^*(\omega)}{Z_c^*(\omega)} = \frac{\mathcal{C}_H^*(\omega)}{\mathcal{C}_c^*(\omega)}.$$

The difference on the surface impedances are even more enhanced due to the $\cot(k(\omega)d)$ term. Thus significant modifications have to be expected in the reflection and absorption properties within and around the band gap of the media.

Remark. Conversely to conventional waves where progressive phase is associated with attenuation, in the atypical band, the *phase* velocity is negative (regressive phase) along with the fact that the wave is attenuated. This feature has been mentioned in [26]. This means that for media exhibiting a negative effective bulk modulus, the energetic consistency imposes that the direction of propagation is determined by the direction of attenuation instead of the direction of progressive phase.

3. Prototypes and experiments

3.1. Design of prototypes

To evidence the unconventional effects described by the theory, we realized several prototypes of porous media with inner resonance. In this view, we have build the three types of materials investigated theoretically, all realized with a common generic structure, namely:

- conventional media (Section 2.2) constituted by a packing of impervious hollow spheres,
- media with resonators (Section 2.3), made of the same sphere packing, however the spheres are perforated and inner ducts are positioned,
- porous matrix with embedded resonators (Section 2.4), realized by filling the inter-sphere pores of the previous prototype by a granular medium having a characteristic size smaller than the spheres.

To highlight the differences between conventional and unconventional media we design the resonators in such a way that their resonance occurs in the frequency range 100–500 Hz where the conventional materials are not efficient for sound absorption. In addition the granular medium has been chosen so that the co-dynamic condition is fulfilled.

For different practical reasons, the radius of the spheres is 20 mm, which enables hand-made Helmholtz resonators with convenient size of the inner duct. For simplicity also, the porous matrix embedding the resonators has been made of rice grains. The design of the arrangement has been guided by the 100 mm diameter of the Kundt's tube used for the experiments. The details of the design are described hereafter.

3.1.1. Sphere packing

The common generic structure is made of four layers of hollow spheres (impervious or resonating) each having a radius $R = 20$ mm. Each layer, is composed of four spheres symmetrically arranged around a 10 mm radius impervious cylinder to reach the 100 mm diameter required by the experimental setup. On two successive layers, the spheres are shifted by an angle of $\pi/4$ to reach the maximum possible compaction. With this common structure made of 16 spheres, all the tested samples are cylindrical samples of 100 mm diameter and 138 mm thick, and consist of two periods. The arrangement is shown in Fig. 5. The porosity of the inter-sphere pore network is calculated as:

$$1 - \phi_p = \frac{16(4\pi/3)2^3 + \pi 13.8}{\pi 5^2 13.8} \quad \text{i.e. } \phi_p = 0.47.$$

The pore geometry defined by this regular packing, can be assimilated to a cubic centered array of spheres having the same porosity, as studied in [22]. According to this work, the intrinsic permeability and the tortuosity can be assessed from self consistent analytical expressions:

$$\mathcal{K}_p \approx \frac{R^2}{3\phi_p^{\frac{2}{3}}}\left[\frac{2+3\phi_p^{\frac{5}{3}}}{\left(2\phi_p^{\frac{5}{3}}+3\right)\phi_p^{\frac{1}{3}}} - 1\right] = 3.7\ 10^{-6}\ \text{m}^2; \qquad \alpha_{p\infty} \approx \frac{3-\phi_p}{2} = 1.27.$$

From these values the critical frequency of the pore network is

$$f_c \approx \frac{1}{2\pi}\frac{\phi_p \mu}{\mathcal{K}_p \rho^e \alpha_{p\infty}} = 0.24\ \text{Hz}.$$

Thus, in the frequency range of usability of the Kundt's tube, namely 50–1900 Hz, the porous network is in inertial regime. Then, according to the analysis of Section 2.3.2, the co-dynamic condition will be necessarily satisfied if impervious spheres are replaced by resonators of eigenfrequency $f_0 = \omega_0/(2\pi)$ falling in the range between 100 and 500 Hz.

Fig. 5. Sphere packing (138 mm high) common to the whole tested configurations described in Table 1. Central cylinder is impervious while spheres might be impervious hollow spheres (M1) or resonators (M2, M3, M5) or both (M4). The inter-spheres space might be occupied either by air (M1–M5) or filled by a granular media (M6). Left: design of prototype, middle: a prototype, right: Cut of the two types of Helmholtz resonators.

Since waves propagate when the pores network behaves in inertial regime, the diffraction frequency associated to the sphere packing defined by $\frac{\Lambda_p(\omega_d)}{2\pi} \approx 2R$ can be assessed by the high frequency velocity estimate. Then,

$$\frac{\Lambda_p(\omega_d)}{2\pi} \approx \frac{1}{2\pi f_d}\frac{\mathcal{C}^e}{\sqrt{\alpha_{p\infty}}} \approx 2R \quad \text{gives } f_d \approx 1200 \text{ Hz}.$$

Consequently, below $f_d/2 = 600$ Hz, the diffraction effects can be disregarded, while small perturbations due to diffraction can be expected in the range of [600–1000] Hz. Now, above this range, the diffraction plays a determining role [27], and the present macroscopic modeling becomes irrelevant. For this reason all the experimental and simulated results are displayed in the [50–1000] Hz range.

3.1.2. Helmholtz resonators

The geometry of the resonators is that described in Fig. 3. Denoting the radius of the duct by αR, the frequency of resonance given by (11) is rewritten

$$f_0 = \mathcal{C}^e \frac{|\Sigma|}{2\pi\sqrt{|\widetilde{\Omega}||\Omega'|}} = \mathcal{C}^e \frac{\sqrt{3}}{4\pi}\frac{\alpha}{\sqrt{R\ell'}}.$$

A series of resonators tuned at two different frequencies have been realized by perforating the hollow spheres and inserting a duct of $\ell' = 15$ mm length and of radius $\alpha_1 R = 0.9$ mm or $\alpha_2 R = 2.3$ mm, see Fig. 5. In both cases the duct section satisfies the condition $|\Sigma|/R^2 \leq 1.5\% \ll 1$. The corresponding frequencies for the tubes of small and larger section are assessed respectively at 123 Hz and 314 Hz.

In reality these design values should (slightly) overestimate the actual values. In fact, since the velocity in the duct differ from that in the chamber and in the pores, there is a transition zone in the vicinity of the duct apertures which enables the matching of both fields. In practice, it is known that this region is of the order of the radius of the duct (which therefore presents an effective length slightly longer than its actual length). For design purposes, this effect can be disregarded. Indeed if instead of ℓ' we consider an apparent additional length on both extremities i.e. $\ell' + 2\alpha R$ the assessed frequencies would becomes 115 and 272 Hz.

With these dimensions one can check that the viscosity effect on the moving mass in the duct is not significant in the range of the resonant frequency. Indeed, the gas flow is governed by inertia when angular frequencies are significantly higher than the critical visco-inertial frequency f_c' of the duct. This latter reads classically $f_c' = 8\mu/(2\pi\rho^e(\alpha R)^2)$. Thus, at the resonant frequency:

$$\frac{f_0}{f_c'} = \frac{\mathcal{C}^e\rho^e}{\mu}\frac{\sqrt{3}}{16}\alpha^3 R\sqrt{\frac{R}{\ell'}} \approx 2.4\times 10^6\alpha^3 R\sqrt{\frac{R}{\ell'}}.$$

For the resonators tuned at 123 and 314 Hz, we have respectively $f_0 \approx 5\times f_c'$ and $f_0 \approx 85\times f_c'$, that indicates in any cases a weak viscous dissipation and dominant effects of inertia in the ducts, (with much lower dissipation for the 314 Hz-resonator). Hence, the exact expression of $\tau'(\omega)$ that involves Bessel functions [28,29] can be approximated by $\tau'(\omega) \approx 1 + 1/\sqrt{2i\omega/\omega_c'}$.

3.1.3. Hosting porous matrix

The porous matrix embedding the resonators is constituted by grains of rice cautiously showered on the sphere packing to fill the whole interstitial space around the spheres. The oblong rice grain form, of about 3 mm long, avoids the penetration of

Table 1
Tested materials ; "Imp" stands for impervious spheres. All configurations are based on the sphere packing depicted in Fig. 5 with the same thickness of 138 mm.

Material	Spheres	Host	αR (mm)	c	ϕ
M1	Imp.	Air	–	0	$\phi_p = 0.47$
M2	@123 Hz	Air	0.9	0.53	$\phi_p = 0.47$
M3	@314 Hz	Air	2.3	0.53	$\phi_p = 0.47$
M4	Imp. + @314 Hz	Air	2.3	– ; 0.265	$\phi_p = 0.47$
M5	@123 Hz + @314 Hz	Air	0.9/2.3	0.265 ; 0.265	$\phi_p = 0.47$
M6	@314 Hz	Porous	2.3	0.53	$\phi_m = 0.40$

the grains into the resonators. The grain radius is approximately 1 mm, much smaller than the sphere radius. So the granular filling appears as a continuous porous medium at the scale of the spheres. From simple density measurements the porosity of the matrix is assessed to be $\phi_m = 0.40$. In order to check the feasibility, rough assessments of the matrix permeability, tortuosity and critical frequency are given by the self consistent estimates, (using the grain radius despite the oblong form of grain, to better account for the inter-grain pore size). This yields:

$$\mathcal{K}_m \approx 2.9\,10^{-8}\ \mathrm{m}^2; \qquad \alpha_{m_\infty} \approx 1.3; \qquad f_{c_m} \approx \frac{1}{2\pi}\frac{\phi_m \mu}{\mathcal{K}_m \rho^e \alpha_{m_\infty}} = 30\ \mathrm{Hz}.$$

Hence, for frequencies between 100 and 500 Hz, the porous matrix should behave in inertial regime and the co-dynamic condition (Section 2.3.2) is fulfilled. Nevertheless, this conclusion is based on rough estimates and have to be checked experimentally. More generally the basic parameters of the three constituents will be reevaluated independently from the measurements (Section 4.1).

3.2. Configurations and experiments

Using the above designed constituents, six different configurations corresponding to a conventional porous medium and 5 meta-porous media were tested, namely: the stack of impervious spheres (M1), stacks of resonators tuned at two different frequencies (M2–M3), a stack of resonators mixed with impervious spheres (M4), a stack of mixed resonators at two different frequencies (M5) and a stack of resonators embedded in a porous medium (M6). The materials were filled with air at ambient temperature, pressure and humidity conditions. These configurations are listed in Table 1. A series of experimental tests have been carried out on the different materials, with three main objectives:

- to determine experimentally the actual acoustic parameters of the two conventional media, i.e. impervious sphere packing and porous matrix, that enables comparisons with unconventional media,
- to provide measurements of the dynamic permeability and of the effective bulk modulus in both conventional and non conventional media, in order verify the actual influence of the inner resonance on both parameters. These two quantities also enable computing the anomalous dispersion of sound velocity and attenuation,
- to evidence the atypical sound absorption properties and to check the model validity by comparing measured data against simulated results.

These issues are addressed through two types of measurements performed at ambient conditions of pressure, temperature and humidity, with the Kundt's tube facilities (100 mm diameter) available at the laboratory of ENTPE.

Surface properties have been measured according to the procedure recommended in ISO 10534-2 [30]. This has the advantage to correspond to well controlled test conditions and to allow for small size samples to be tested in the wide frequency range [50–1900] Hz. Due to the perturbations induced by diffraction, only measurements up to 1000 Hz are presented and discussed. Hence, reflection coefficient, surface impedance and sound absorption coefficient at normal incidence were retrieved.

In addition to these surface properties, the intrinsic characteristics of the sound wave propagation were measured following the procedure described in [31,32]. According to this work, a third microphone is mounted flush in the rigid termination in order to determine the acoustic energy which is transmitted through the tested material. In the present experiments, a length corresponding approximately to the tube diameter was set between the rear side of the material and the rigid termination to ensure that a plane wave behavior is recovered at the third microphone position. Using this procedure, the dynamic permeability (and the effective mass density) as well as the effective bulk modulus were determined.

4. Results: experiments versus theory

4.1. Parameters of the conventional porous media

In view of performing numerical simulations of the inner resonance media with relevant parameters, the acoustic properties of the two conventional porous media (impervious spheres packing and rice grain porous media) were measured. In Fig. 6, the measured sound absorption is compared to simulation obtained by matching the four parameters (the porosity

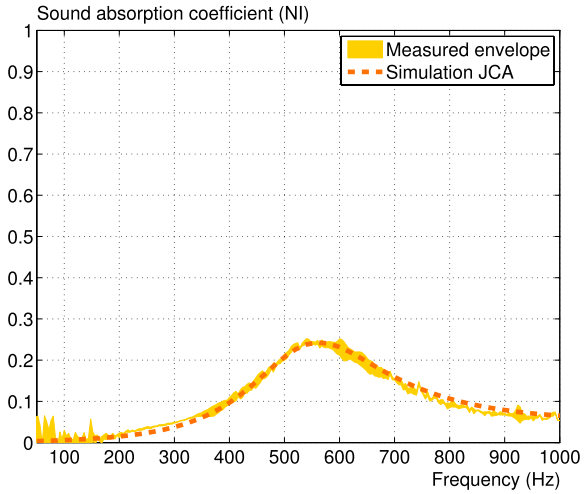

Fig. 6. Sound absorption coefficient of the impervious spheres packing (Fig. 5, material M1 thickness of 138 mm) at ambient conditions of temperature and pressure. Measurements (tick line) and simulation (dashed line) with matched parameters (Color online).

is known) of the Johnson–Champoux–Allard model [25,18]. These parameters have been adjusted based on the prior self-consistent estimations derived in Section 3.1.1. The permeability and tortuosity values used in the present simulation were respectively 2.3×10^{-6} m^2 and 1.4 compared to respectively 3.5×10^{-6} m^2 and 1.3 previously estimated. The viscous and thermal characteristic lengths were set according to the pores geometry, namely the smallest and largest characteristic dimensions of the stack 3 mm and 10 mm. With these values, a good correspondence with the measured data of sound absorption is achieved. The actual critical frequency, $f_c = 0.34$ Hz, is almost the same as the estimated value. Thus, the pore network behaves in inertial and (quasi)-adiabatic regime at the eigen frequencies of the resonators. In addition, the maximum absorption is only of 0.25 and occurs at 550 Hz that approximately corresponds to the quarter wavelength resonance of the material (525 Hz).

The same inversion procedure has been applied to the rice grain porous media. Consistently with the more complex pore geometry, the matched permeability and tortuosity departs from the rough estimates, and take the values $\mathcal{K}_m = 3\,10^{-9}$ m^2; $\alpha_{m_\infty} = 1.7$. The viscous and thermal characteristic lengths, determined by matching the absorption curve are of 0.2 mm and 0.5 mm respectively. These values are in good agreement with the granular medium characteristic dimensions. The critical frequency is higher than previously estimated $f_{c_m} = 200$ Hz, but still fulfills the co-dynamic conditions since, for the designed resonators, $f_{c_m} = O(f_0)$. However, the porous matrix behaves in visco-inertial regime at the resonators resonance.

4.2. Dynamic permeability and effective bulk modulus

The model predicts that the macroscopic effect of the resonators appears on the mass balance, whereas it does not affect the dynamic Darcy's law. As a consequence, the inner resonance phenomenon is "condensated" in the effective bulk modulus that becomes unconventional, while the dynamic permeability (or effective density) keeps its conventional features.

This essential aspect can be directly checked through the measurements of both effective parameters according to the procedure described on Section 3.2. Such tests were performed on materials M1 (conventional) and then on M2 and M4 (inner resonance). As they all present the same pore geometry defined by the common sphere packing, the dynamic permeability should be the same, but the effective bulk modulus should differ. In the studied frequency range, since the sphere packing behaves in inertial regime, it is more convenient to consider the effective density than the dynamic permeability. The experimental data are reported in Figs. 7 and 8.

Firstly, as expected and independently of the inner resonance phenomena, one notices on both parameters the emergence of the typical diffraction effects (see [33,27,34]) at frequency around 500 Hz, the deviations from the conventional model becoming significant around 1000 Hz. Thus, this phenomenon is sufficiently separated in frequency and does not interfere with the inner resonance effect. Note also that the three material present an unexpected perturbation at 375 Hz, which is therefore an effect of the pore network.

Secondly, in the range of weak diffraction effect, the experiments clearly confirm the theoretical prediction: the effective density is not affected by the presence of the resonators or a mix of resonators and impervious spheres and remains identical to conventional effective density for frequencies lower than 500 Hz. Conversely, the bulk moduli differ for three inner resonance materials and depart significantly from the conventional modulus of the impervious spheres packing.

According to the theory, the atypical frequency variation of the bulk modulus are directly related to the eigen frequency and the concentration of resonator of each material. The signature of the resonance, with a decrease of the bulk modulus immediately followed by a rapid increase is observed for the inner resonant materials studied here. These effects are very

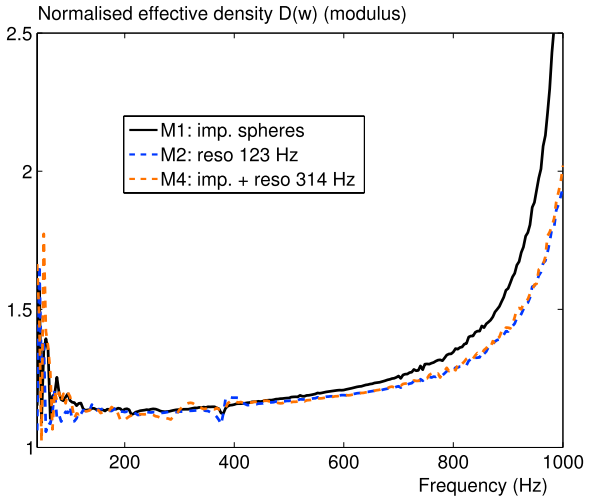

Fig. 7. Modulus of the effective density of materials M1 (conventional), M2 and M4 (inner resonance). Normalization by ρ^e/ϕ_p. (Color online).

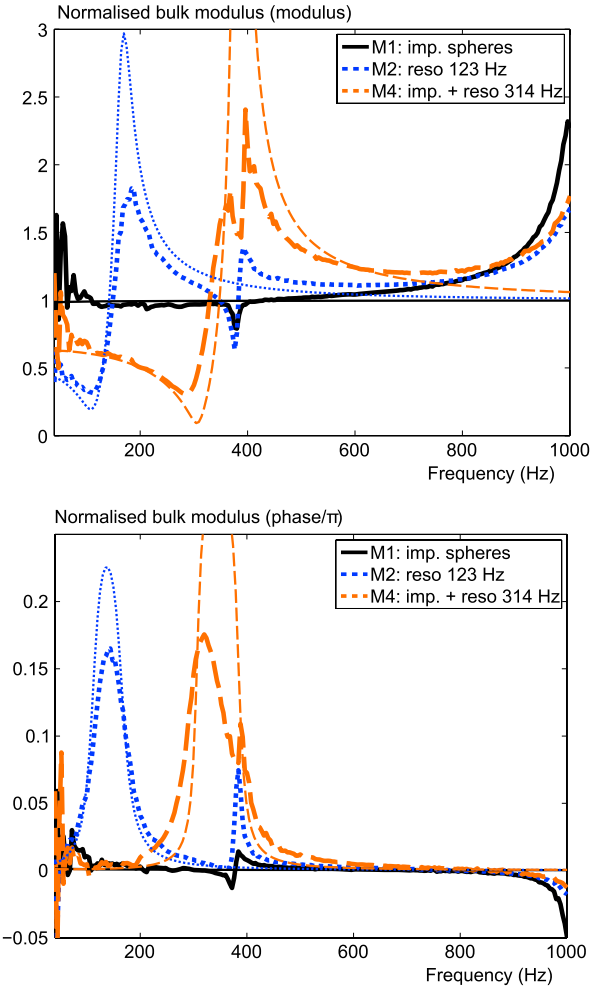

Fig. 8. Effective bulk modulus of materials M1 (conventional), M2 and M4 (inner resonance). Experimental data (thick line) versus simulations with *a priori* parameters (thin line). Top: Modulus normalized by the adiabatic bulk modulus of the pore network $\gamma P^e/\phi_p$, Down: Phase/π (Color online).

Table 2
A priori and *matched* parameters of the resonators.

	Resonator 1 used in M2, M4		Resonator 2 used in M3, M4, M5, M6	
Parameters	*a priori*	*matched*	*a priori*	*matched*
$f_0(\ell')$	123 Hz	116 Hz	314 Hz	282 Hz
$f_0(\ell'+2\alpha R)$	115 Hz		272 Hz	
f_c'	25 Hz	–	4 Hz	–
ξ	$\sim 2\times 10^{-4}$	$3\times 10^{-4}=\xi_2$	$\sim 1.5\times 10^{-5}$	$5\times 10^{-5}=\xi_3$

significant, in particular the minimum/maximum magnitude could be up to one order smaller/higher than that of a standard porous medium. Furthermore the perturbations concern a wide frequency range of about 300 Hz. The simulation of the effective bulk modulus derived theoretically (Eq. (25)), simplified according to the inertial and (quasi)-adiabatic regime and computed with the "a priori" estimated parameters of the resonators of materials M2 and M4 i.e.,

$$E(\omega)=\gamma P^e\left(\phi_p+\frac{c}{1-(\omega/\omega_0)^2(1+1/\sqrt{2i\omega/\omega_c'})}\right)^{-1}$$

are presented in Fig. 8. The simulations are in good qualitative agreement with the experiments. At the resonator resonance, the bulk modulus reaches a minimum which corresponds to the maximum of the resonator response (disregarding the slight shift due to dissipation). However, the magnitude of the variations is overestimated. This indicate an underestimation of the damping, meaning that other(s) dissipation mechanism(s) than the slight viscous effects on the duct are involved in the behavior of the resonator. This mismatching may be related to a viscous resistance encountered by the resonator flow at the pores aperture. This effect is not described by the theory at the leading order and remains to be investigated by introducing correctors, such as next order expansion terms and/or matched expansions in the transition zones. Nevertheless, this leads to consider that the actual resonator behavior is likely governed by a transfer function of the classical type $1-(\omega/\omega_0)^2+2i\xi\omega$ (instead of $1-(\omega/\omega_0)^2(1+1/\sqrt{2i\omega/\omega_c'})$), where ξ accounts for the viscous dissipation.

$$E_{exp}(\omega)=\gamma P^e\left(\phi_p+\frac{c}{1-(\omega/\omega_0)^2+2i\xi\omega}\right)^{-1}. \tag{38}$$

Then, using expression (38), the experimental curves enable to identify the actual resonance parameters of the resonators. This leads to consider for materials M2 and M4, a resonance at 116 Hz, respectively 284 Hz, and a damping factor $\xi = 3\times 10^{-4}$, respectively $\xi = 5\times 10^{-5}$. In the sequel, the "a priori" parameters indicates ω_0 and ω_c' issued from "a priori" estimations, while "matched" parameters indicate ω_0 and ξ, derived from effective bulk modulus measurements. The different values are indicated in Table 2 (the equivalent damping of the resonator at ω_0 is indicated with a $\sim$). The Table shows that the observed eigen-frequencies are close to the "a priori" values with corrected duct length, and confirms the underestimation of the weak damping. Using these matched values, the correspondence between the experimental and simulated moduli is satisfactory in the frequency range unaffected by the diffraction, see Fig. 9.

4.3. Features of wave propagation

From the effective parameters determined experimentally, the complex wave velocity is computed and the modulus and phase are displayed in Fig. 10. As the effective densities vary smoothly, the anomalies on wave properties are directly inherited from those of the effective bulk modulus. The inner resonance induces two main effects:

- a non monotonic dispersion of the velocity modulus, with significant variation (more than 50%) compared to conventional materials,
- a phase reaching values as $\pi/4$, indicating a huge increase of attenuation in the same frequency range.

This high level of attenuation is consistent with the band-gap occurrence. Nevertheless, due to the dissipation, the band gap is smoothed in a transition zone instead of being sharply confined in frequency. In practice, the nature of the wave propagation shifts from standard (quasi-)hyperbolic waves to highly damped waves confined on the surface. In this regime, because of both changes in velocity and attenuation, the characteristic impedance is drastically modified. This results in two opposite effects on energy absorption: the highest impedance contrast may reduce the wave penetration, while the high attenuation may enhance the dissipation. The actual absorption described in the next section results from the combination of these two effects.

4.4. Sound absorption

Conversely to the effective parameters, the sound absorption is not strictly an intrinsic property of the material, since the geometrical configuration of the test is involved. Nevertheless, beside the previous model validation, it is of interest to

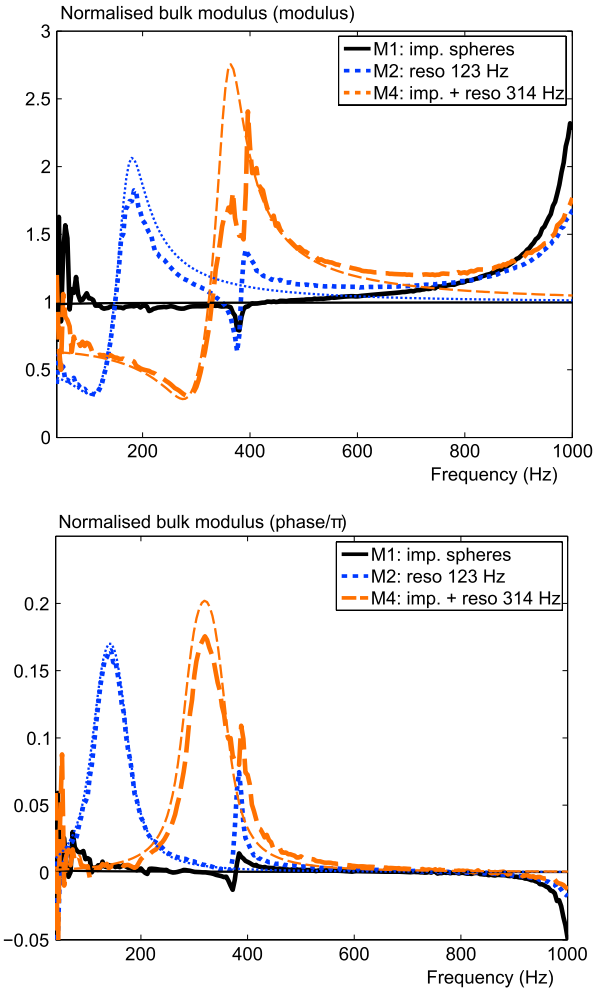

Fig. 9. Effective bulk modulus. Experimental data versus simulations with *matched* parameters (thin line). Same legend as Fig. 8 (Color online).

highlight the unusual absorption properties through experiments performed on the six media M1–M6 in identical configuration, i.e. material of 138 mm thick in contact with an impervious backing. Moreover, the comparison of measurements and simulations provide additional information to validate or to improve the theoretical model.

4.4.1. Media made of resonators

Fig. 11 displays the sound absorption coefficient measured (thick lines) and simulated (thin lines) for the materials M2 and M3 made of the two types of resonators. This figure deserves several comments.

The drastic difference with the conventional material M1 made of impervious spheres (see Fig. 6) is noticeable, especially around the eigen frequencies of the resonators. The significant increase of absorption demonstrates the interesting potential of meta porous media for practical purposes.

The presence of band-gap is not contradictory with an absorption effect. Indeed band-gap means that in the depth of the material the wave necessarily vanishes and therefore its propagation is avoided. However, for media of finite thickness, the evanescent wave does exist on a boundary layer in which the energy is dissipated. Thus, in the band-gaps, the energy balance has to account for this surface energy. Consequently, meanwhile the transmitted wave vanishes, the incident wave is only partially reflected instead of being perfectly reflected.

For material M2 (a priori tuned at 120 Hz) the effect of the resonator disappears above 400 Hz (see Fig. 8), and the second absorption peak around 550 Hz, is identical in frequency and magnitude to that of the impervious sphere material M1. For material M3 (a priori tuned at 314 Hz) the effect of the resonator subsists up to 600–700 Hz (see Fig. 8), and interacts with the quarter wavelength resonance of the sphere arrangement. Such a combination of local and global resonance results in a large enhancement of absorption (compared to M1) in this frequency range, and in a shift of the peak frequency from 550 to 630 Hz. This situation presents strong similitude with the meta-surface effect already noticed in elasticity [35,36].

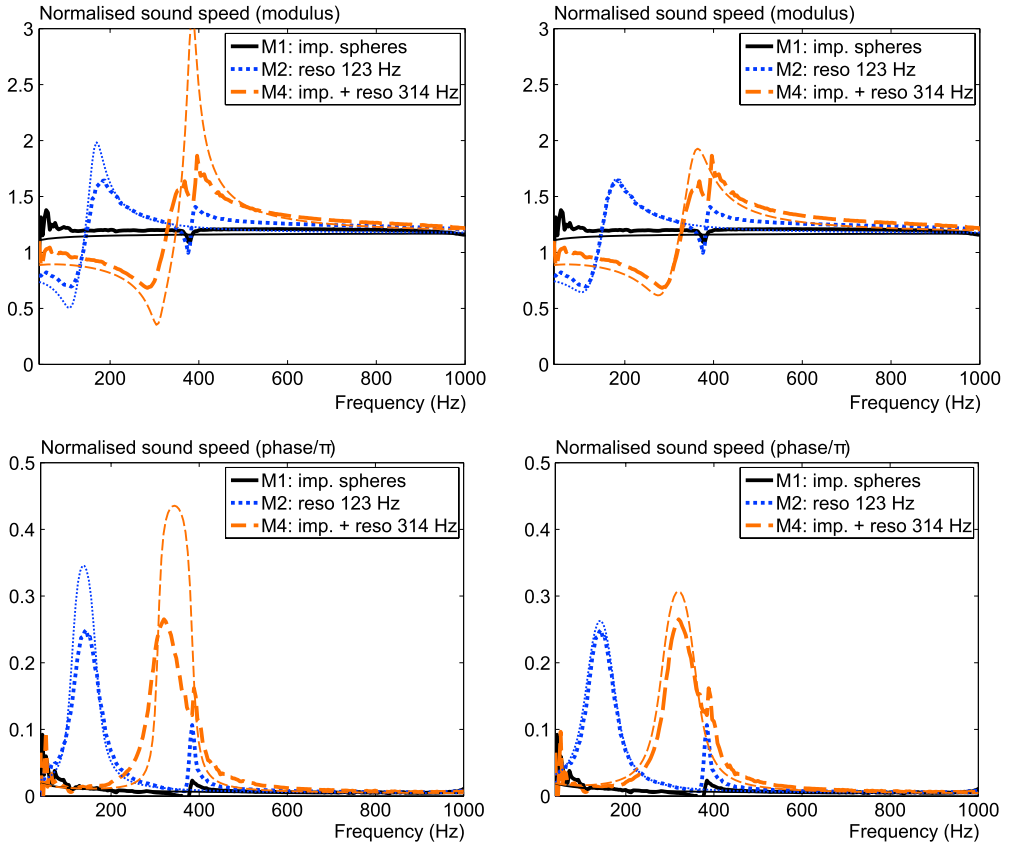

Fig. 10. Sound velocity (modulus on top line, phase on bottom line) of materials M1 (conventional) and M2, M4 (inner resonance). Experimental data (thick line) versus simulations (thin line) with *a priori* parameters (on left); with *matched* parameters (on right). Normalization by the sound velocity c^e (Color online).

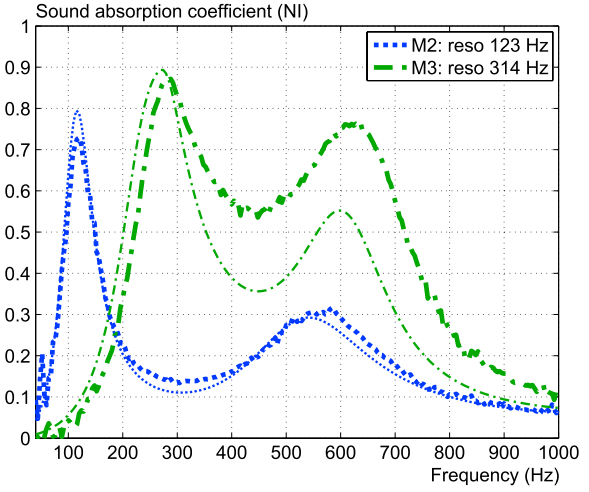

Fig. 11. Sound absorption coefficient at normal incidence of materials M2 and M3 made of resonators tuned at 123 Hz and at 314 Hz. Experimental data (thick line) versus simulations with *matched* parameters (thin line) (Color online).

These experimental data have been simulated using two sets of parameters:

- those given by "a priori" parameters (with formula (25) for effective bulk modulus),
- the "matched" parameters identified with the bulk modulus measurement (together with formula (38) for the effective bulk modulus).

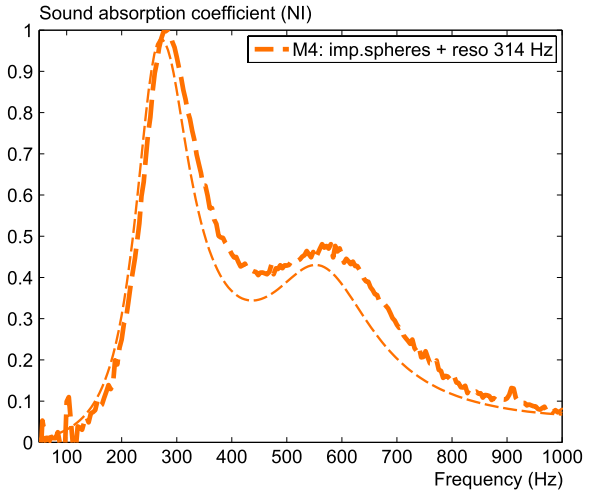

Fig. 12. Sound absorption (at normal incidence) of material M4 made of resonators a priori tuned at 314 Hz and impervious spheres in identical proportion. Experimental data (thick line) versus simulations with *matched* parameters (thin line) (Color online).

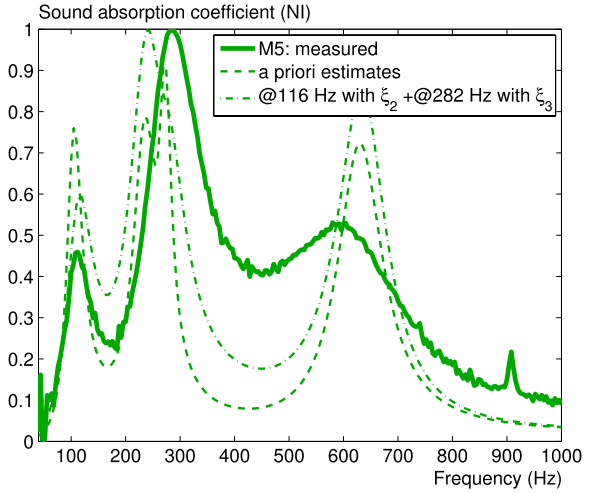

Fig. 13. Sound absorption (at normal incidence) of material M5 made of resonators a priori tuned at 123 and 314 Hz in identical proportion. Experimental data (thick line) versus simulations with *a priori* (dot line) and *matched* parameters defined in Table 2 (dash dot line), (Color online).

For both media, the "a priori" simulations correctly retrieve the qualitative form of the absorption curves, in particular the frequencies of maximum absorption are well predicted. A quantitative agreement is also observed for the absorption peak related to the inner resonance. Quantitatively, off the two resonances, simulated results exhibit an absorption level lower than the measured one. This observation is consistent with the under-estimation of the resonator dissipation previously mentioned. This assumption is supported by the "matched" simulations that correctly reproduce the experimental data.

4.4.2. Mix of impervious spheres and/or resonators

The above comments also apply to mixed media M4 and M5.

For media M4, made of equal proportion of resonator and impervious spheres, measured and predicted data with "a priori" and "matched" parameters are displayed in Fig. 13. Compared with the absorption of media M3, Fig. 11, the experimental results evidence the higher influence of the resonators when they are in higher concentration, especially around the quarter wavelength resonance which is observed around 590 Hz. It is likely that the dissipation inside the resonator is responsible for this lack of dissipation in the model. The simulations also confirm the qualitative agreement of the model with the "a priori" estimates (the frequencies of the two main peaks are correct, while the absorption is significantly under-estimated); and the reasonably correct description with the "matched" parameters corresponding to enhanced resonator dissipation.

Fig. 12 displays the measured and predicted data for media M5 made of equal proportion of the two types of resonators. These data disclose the cumulative effect of the resonators, each type providing a large absorption around its eigen frequency. The simulations realized using the effective bulk modulus expression (32) with "a priori" and "matched" parameters gives respectively good qualitative and quantitative descriptions.

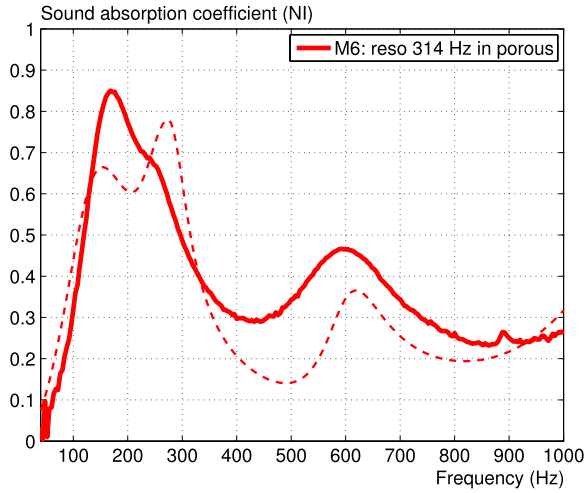

Fig. 14. Sound absorption (at normal incidence) of material M6 made of resonators a priori tuned at 314 H embedded in a porous matrix. Experimental data (thick line) versus simulations with *matched* parameters (thin line) (Color online).

4.4.3. Resonators embedded in porous media

The last configuration M6 corresponds to resonators a priori tuned at 314 Hz embedded in a porous medium. Measured and simulated data (with "a priori" and "matched" parameters) are compared in Fig. 14. The main difference between the previous cases is that the matrix behaves in visco-inertial regime ($f_{cm} = 200$ Hz) at the resonator eigen frequency. This induces more complicated effect because both matrix and resonator have complex moduli that vary significantly with frequency. As a result, in place of the single peak due to the resonators a priori tuned at 314 Hz, two separate peaks are visible around 170 and 250 Hz. These two peaks are also predicted by the model and, more generally, a good correspondence is observed in the whole frequency range between simulations and experiments. Note that the deviation due to the underestimated level of dissipation is reduced when embedding the resonators in a dissipative porous medium.

To sum up, the principle of the model and its main outcomes are confirmed by a series of experiments performed on several materials. The model is reliable, at least for a preliminary design of unconventional porous media. The weak point lies in the under estimation of the dissipation, and improvements on this aspect are currently investigated.

5. Conclusion

In this paper, it is demonstrated analytically and illustrated experimentally that inserting insert resonators (possibly of different nature) in porous media leads to effective acoustic properties that depart significantly from conventional poro-acoustic. This relies on the occurrence of a "co-dynamic" regime, in which macro wavelengths and local resonance occur simultaneously. Indeed, in the inner-resonance frequency range, the elasto-inertial response of the resonator acts as a complex and possibly negative bulk modulus, which induces an effective negative stiffness of the porous media in a "atypical" frequency band. Thus, the features of acoustic wave are drastically modified, especially within and around this atypical band, that corresponds to a low frequency band gap. The "co-dynamic" regime is a specific situation that departs from:

- Rayleigh scattering where wavelengths are larger than the period, so that local dynamic effects are weak,
- Bragg scattering at high frequency where wavelengths comparable to the array's size [37], so that band gaps are strictly related to diffraction, see e.g. [38,13].

However, it should be possible to consider the "co-dynamic" regime as a particular case of recently developed theories as the non local theory established in [12,39], or the high frequency modulation approach, e.g. [40,41], derived through asymptotic expansions in the Floquet–Bloch framework.

The present multi-scale analysis of inner-resonant porous media leads, at the leading order, to an analytic formulation where the effective parameters are fully determined from the knowledge of the geometry and of the properties at the period scale. Thus, the model can easily be used to design unconventional acoustic media.

Such ability has been developed in practice and has lead to several prototypes. A series of experiments confirm the main theoretical outcomes, in particular the high absorption at low frequency of the designed materials. It is worth mentioning that this high absorption is obtained with materials made of hollow spheres having a total density of 4.2 kg/m^3 (without granular matrix), i.e., less than 4 times the air density, having a total porosity of 0.998, i.e., only 2 thousand of the volume is occupied by the solid, but being nevertheless sufficiently stiff to appear as rigid for airborne sound excitation.

This demonstrates that inner resonant porous media can be simply realized in laboratory but also at industrial scale. They present practical interest for engineering acoustic applications, that may concern the design of new systems, either for

damping (large absorption at low wavelengths) or for fast/low velocity purposes (acoustic mirages or acoustic decoys), at different spatial and/or frequency scales.

Further theoretical and experimental works are in progress (i) to improve the model with correctors involving higher order terms in the expansions and/or matched expansions in the transition zones, (ii) to investigate various resonator configurations (thickness, sound incidence etc.) and (iii) other types of resonators. In addition, the sound transmission properties are currently investigated to assess materials having low dissipation properties and high dispersion capacity.

Acknowledgments

We thank F. Sallet from ENTPE for his help in realizing prototypes and experiments and F. Chevillotte from Matelys for the model implementation. This work was performed within the framework of the Labex CeLyA of Université de Lyon, operated by the Agence Nationale de La Recherche (ANR-10-LABX-0060/ANR-11-IDEX-0007).

References

[1] J.-L. Auriault, G. Bonnet, Dynamique des composites élastiques périodiques, Arch. Mech. 37 (4–5) (1985) 269–284.
[2] J.-L. Auriault, C. Boutin, Long wavelength inner-resonance cut-off frequencies in elastic composite materials, Int. J. Solids Struct. 49 (2012) 3269–3281.
[3] J.O. Vasseur, P.A. Deymier, G. Prantziskonis, G. Hong, Experimental evidence for the existence of absolute acoustic band gaps in two-dimensional periodic composite media, J. Phys.: Condens. Matter. 10 (1998) 6051–6064.
[4] Z. Liu, X. Zhang, Y.Y. Mao, Z. ZHU, C.T. Yang, Chan P. Sheng, Locally resonant materials, Science 289 (2000) 1734–1736.
[5] P. Sheng, X.X. Zhang, Z. Liu, C.T. Chan, Locally resonant sonic materials, Physica B 338 (2003) 201–205.
[6] J.-L. Auriault, C. Boutin, Deformable porous media with double porosity. III acoustics, Transp. Porous Media 14 (1994) 143–162.
[7] C. Boutin, P. Royer, J.L. Auriault, Acoustic absorption of porous surfacing with dual porosity, Int. J. Solids Struct. 35 (34–35) (1998) 4709–4737.
[8] X. Olny, C. Boutin, Acoustic wave propagation in double porosity media, J. Acoust. Soc. Am. 113 (6) (2003) 73–89.
[9] G. Pispola, K.V. Horoshenkov, A. Khan, Comparison of two modeling approaches for highly heterogeneous porous media, J. Acoust. Soc. Am. 121 (2) (2007) 961–966.
[10] C. Chesnais, C. Boutin, S. Hans, Effects of the local resonance on the wave propagation in periodic frame structures: generalized Newtonian mechanics, J. Acoust. Soc. Am. 132 (4) (2012) 2873–2886.
[11] C. Boutin, Acoustics of porous media with inner resonators, J. Acoust. Soc. Am. 134 (6) (2013) 4717–4730.
[12] D. Lafarge, N. Nemati, Nonlocal Maxwellian theory of sound propagation in fluid-saturated rigid-framed porous media, Wave Motion 50 (2013) 1016–1035.
[13] H. Pichard, O. Richoux, J.-P. Groby, Experimental demonstrations in audible frequency range of band gap tunability and negative refraction in two-dimensional sonic crystal, J. Acoust. Soc. Am. 132 (4) (2012) 2816–2822.
[14] E. Sanchez Palencia, Nonhomogeneous Media and Vibration Theory, in: Lectures Notes in Physics, vol. 127, Springer-Verlag, Berlin, 1980, p. 398.
[15] J.-L. Auriault, C. Boutin, C. Geindreau, Homogenization of Coupled Phenomena in Heterogenous Media, ISTE and Wiley, 2009.
[16] J.-L. Auriault, Dynamic behaviour of a porous medium saturated by a Newtonian fluid, Internat. J. Engrg. Sci. 18 (1980) 775–785.
[17] K. Attenborough, Acoustical characteristics of rigid fibrous absorbents and granular media, J. Acoust. Soc. Am. 73 (3) (1983) 785–799.
[18] Y. Champoux, J.F. Allard, Dynamic tortuosity and bulk modulus in air saturated porous media, J. Appl. Phys. 70 (1991) 1975–1979.
[19] J.-L. Auriault, L. Borne, G. Chambon, Dynamics of porous saturated media, checking of the generalized law of Darcy, J. Acoust. Soc. Am. 77 (1985) 1641–1650.
[20] D. Lafarge, P. Lemarinier, J.-F. Allard, V. Tarnow, Dynamic compressibility of air in porous structures at audible frequencies, J. Acoust. Soc. Am. 102 (1997) 1995–2006.
[21] Z. Hashin, Assessement of the self consistent scheme approximation: conductivity of particulate composite, J. Comput. Math. 2 (1968) 284.
[22] C. Boutin, C. Geindreau, Periodic homogenization and consistent estimates of transport parameters through sphere and polyhedron packings in the whole porosity range, Phys. Rev. E 80 (2010) 036313-18.
[23] P. Leclaire, T. Dupont, R. Panneton, Acoustics of porous materials with partially opened porosity, J. Acoust. Soc. Am. 134 (2013) 4630–4641.
[24] R. Venegas, O. Umnova, Acoustical properties of double porosity granular materials, J. Acoust. Soc. Am. 130 (5) (2011) 2765–2776.
[25] D.L. Johnson, J. Koplik, R. Dashen, Theory of dynamic permeability and tortuosity in fluid-saturated porous media, J. Fluid Mech. 176 (1987) 379–402.
[26] N. Fang, D. Xi, J. Xu, M. Ambati, W. Srituravanich, C. Sun, X. Zang, Ultrasonic meta-material with negative modulus, Nature Mater. 5 (2006) 452–456.
[27] V. Tournat, V. Pagneux, D. Lafarge, L. Jaouen, Multiple scattering of acoustic waves and porous absorbing media, Phys. Rev. E 70 (2004) 026609:1-9.
[28] C. Zwikker, W. Kosten, Sound Absorbing Materials, Elsevier, Amsterdam, 1949, p. 300 (Chapter 2).
[29] M.A. Biot, Theory of propagation of elastic waves in a fluid-saturated porous solid. I. Low-frequency range, II. Higher frequency, J. Acoust. Soc. Am. 28 (1956) 168–178. 179–191.
[30] EN ISO 10534-2 Acoustics — determination of sound absorption coefficient and impedance in impedance tubes — part 2: Transfer-function method, International Organization for Standardization, Geneva, 1991.
[31] T. Iwase, Y. Izumi, R. Kawabata, A new measuring method for sound propagation constant by using sound tube without any air spaces back of a test material, in: Proceedings of inter.noise 98, Christchurch, New Zealand, 1998.
[32] F. Chevillotte, L. Jaouen, F.-X. Bécot, Modèle visco-thermique de matériaux poreux hétérogènes et ses applications, in: Proceedings of CFA 2014, Poitiers, France, 2014.
[33] P. Leclaire, L. Kelders, W. Lauriks, C. Glorieux, J. Thoen, Determination of the viscous characteristic length in air-filled porous materials by ultrasonic attenuation measurements, J. Acoust. Soc. Am. 99 (1996) 1944–1948.
[34] C. Boutin, Rayleigh scattering of acoustic wave in rigid porous media, J. Acoust. Soc. Am. 12 (4) (2007) 1888–1905.
[35] C. Boutin, P. Roussillon, Assessment of the urbanization effect on seismic response, Bull. Seismol. Soc. Am. 94 (1) (2004) 251–268.
[36] L. Schwan, Etude théorique et expérimentale de surface résonantes en milieu élastique (Ph.D. thesis), ENTPE, Lyon, France, 2014, p. 317.
[37] L. Brillouin, M. Parodi, Wave Propagation in Periodic Structures, McGraw-Hill, New York, 1946, p. 272.
[38] A. Krynkin, O. Umnova, Y.B.A. Chong, S. Taherzadeh, K. Attenborough, Scattering by coupled resonating elements in air, J. Phys. D: Appl. Phys. 44 (2011) 125101.
[39] N. Nemati, D. Lafarge, Check on a nonlocal Maxwellian theory of sound propagation in fluid saturated rigid-framed porous media, Wave Motion 51 (2014) 716–728.
[40] R.V. Craster, J. Klapunov, A.V. Pichugin, High-frequency homogenization for periodic media, Proc. R. Soc. A 466 (2010) 2341.
[41] C. Boutin, A. Rallu, S. Hans, Large scale modulation of high frequency acoustics waves in periodic porous media, J. Acoust. Soc. Am. 113 (6) (2012) 73–89.